

Perception-aware Sampling for Scatterplot Visualizations

Zafeiria Moumoulidou
University of Massachusetts Amherst
zmoumoulidou@cs.umass.edu

Hamza Elhamdadi
University of Massachusetts Amherst
helhamdadi@umass.edu

Ke Yang
University of Texas at San Antonio
ke.yang@utsa.edu

Subrata Mitra
Adobe Research
sumitra@adobe.com

Cindy Xiong Bearfield
Georgia Institute of Technology
cxiong@gatech.edu

Alexandra Meliou
University of Massachusetts Amherst
ameli@cs.umass.edu

Abstract

Visualizing data is often a crucial first step in data analytics workflows, but growing data sizes pose challenges due to computational and visual perception limitations. As a result, data analysts commonly *down-sample* their data and work with subsets. Deriving representative samples, however, remains a challenge. This paper focuses on scatterplots, a widely-used visualization type, and introduces a novel sampling objective—*perception-awareness*—aiming to improve sample efficacy by targeting humans’ perception of a visualization.

We make the following contributions: (1) We propose *perception-augmented databases* and design PAwS: a novel *perception-aware* sampling method for scatterplots that leverages saliency maps—a computer vision tool for predicting areas of attention focus in visualizations—and models perception-awareness via saliency, density, and coverage objectives. (2) We design APPROPAwS: a fast, perception-aware method for approximate visualizations, which exploits the fact that small visual perturbations are often imperceptible to humans. (3) We introduce the concept of *perceptual similarity* as a metric for sample quality, and present a novel method that compares saliency maps to measure it. (4) Our extensive experimental evaluation shows that our methods consistently outperform prior art in producing samples with high perceptual similarity, while APPROPAwS achieves up to 100× speed-ups with minimal loss in visual fidelity. Our user study shows that PAwS is often preferred by humans, validating our quantitative findings.

1 Introduction

Data visualizations are a powerful tool commonly used by practitioners to understand, analyze, and find interesting patterns in their data. Scatterplots, in particular, are one of the most popular and frequently used visualization types [69, 92, 107]. Their efficiency and usability have been evaluated in various visualization tasks, such as those identified by Amar et al. [7]: from identifying outliers and clusters to correlation trends [43, 84–86, 90].

As the amount of data grows, however, data analysis and visualization become highly challenging [21, 22]. This is often due to limitations in human perception: visual clutter can affect visual perception and comprehensibility of data [36, 68]. Moreover, as data gets larger, rendering times increase [64, 75, 97]. Optimizing the design of a scatterplot by varying visual features (e.g., point size, opacity, or color) [36, 84] can address perception challenges, but does not improve rendering scalability [107].

As a result, data analysts commonly work with samples of the data: *sampling* simultaneously tackles perceptual and interactivity challenges [11, 36, 57, 66]. Unfortunately, deriving *good* samples

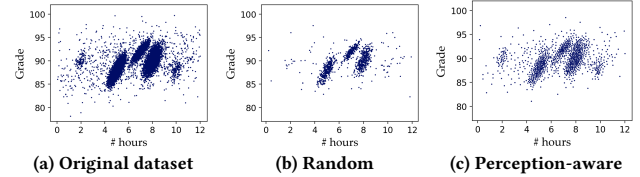


Figure 1: The uniform random sample (b) of the original dataset (a) obscures the presence of the two smaller clusters. A sample of the same size, drawn with our perception-aware sampling method (c), better preserves key features of the original dataset, including trends, clusters, and outlier spread.

is non-trivial. Sampling can introduce artificial data patterns and may fail to represent the underlying information in the data sufficiently. Prior work has identified random sampling as the method most accessible to data analysts in practice [91, 107]. While random sampling is simple, quick, and unbiased, it often fails to reveal underlying patterns in the data or represent corner cases (e.g., outliers).

EXAMPLE 1. *Aysha, a data analyst, is exploring a dataset of historical student performance in three courses offered at a CS program. She uses a scatterplot to analyze the relationship between the time students spend studying per week and their course performance. Aysha draws a sample from the original dataset using uniform random sampling, and gets the visualization of Figure 1b. The visualization supports her expectation that more study time correlates with better grades. However, in this visualization, she fails to notice two separate cohorts of students that would have been clearly visible had she visualized the original data (Figure 1a). The scatterplot of the original data depicts two additional smaller clusters—one indicates students who achieve good grades with little effort, likely due to prior exposure to the course material; the second indicates a small cohort of students who enrolled in the 4-credit section offered by one of the courses, corresponding to higher workload than their peers in the main 3-credit section. These smaller student cohorts are obscured in the sample Aysha is working with, causing her to miss important information and context in the data.*

While working with samples is common in data analytics and visualization, as the example demonstrates, it may also lead to missed critical insights and distorted perceptions of the underlying trends in the data. With a distorted perception of the data, the user may fail at downstream tasks, such as feature selection or model design. *The objective of this work is to design a data selection method that aims to optimize samples for human perception:* given a desired sample size k and a target scatterplot visualization, we want to select k data points such that, when visualized in the target scatterplot, the sample best *captures* key *focal* aspects of the scatterplot of the

original data. Figure 1c depicts the sample that our *perception-aware sampling* method generates on the data of Example 1.

Why YASM (Yet Another Sampling Method)? There is an abundance of sampling techniques, and the relevant literature goes back many decades [9, 11, 14, 22, 37, 52, 57, 65, 74, 75, 83, 87]. Frequently, sampling methods optimize for preserving *data-driven* properties like outliers, relative densities, spatial separation, or data shape [84, 107]. Each method is designed to handle specific use cases, and there is no one-size-fits-all solution. Importantly, even when certain data-driven or statistical properties are preserved in a sample, these properties may still appear distorted as perceived by human users through visualizations when sampling algorithms do not specifically consider human perception as an objective.

We revisit the setting of Example 1, and highlight the behavior of three sampling methods that commonly appear in the visualization literature. Figure 2a visualizes the sample produced by density-biased sampling [74], which *probabilistically* over-samples sparser areas and under-samples denser areas; due to randomization, it may fail to properly represent outlier points despite their high probabilities, and as we see in this result, it behaves similarly to random sampling and also misses the smaller clusters. Parker et al. proposed visualization-aware sampling (VAS) [75] with similar goals to our work, to support efficient visualizations using small samples that maintain a good *visual* representation of a larger underlying dataset. VAS optimizes a visualization-aware loss function: the loss of not including a point in the sample is minimized if one of its close neighbors is in the sample. This leads to good overall shape and coverage, but it is very sensitive to noise, and, as we see in the result of Figure 2b, VAS produces a very poor sample on the data of Example 1. Finally, blue-noise sampling uses a radius r to select points that are at least r far apart from each other [106]. This method randomly selects a candidate point and rejects it if the radius condition is not satisfied. To guarantee the sample will reach the required size, the value of r is dynamically reduced. The adaptive nature of blue-noise sampling affords a more balanced representation between dense and sparse areas (Figure 2c). However, this comes at the expense of a high computational cost: Quadri et al. [84] report running times up to two orders of magnitude worse than alternative approaches; Chen et al. [23] find the method takes up to 27 hours to produce a sample of size $k \approx 6K$ out of 1.56M points; in our analysis, blue-noise took ~ 3.6 hours to generate a sample of size $k = 250$ out of 3.5M data points when the slowest of competing methods needed ~ 5 minutes.¹

A recent study evaluating seven sampling methods by Yuan et al. [107], including blue-noise and density-based methods, suggests that existing algorithms excel at preserving only one or two dimensions of data patterns, such as regional density or outliers. There is a need for a sampling method to holistically account for human perception by preserving many key visual features and visually salient regions in a visualization, which will allow analysts to explore a wider range of data patterns with a sample.

Our work posits that sampling algorithms that account for a measure of *human perception* can produce more effective visualizations that are less likely to distort patterns and trends in the visualized

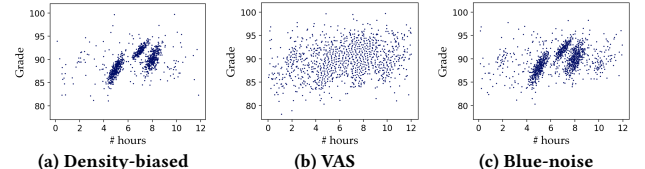


Figure 2: State-of-the-art sampling methods fail to preserve key aspects of the original dataset (Figure 1a). The two smaller clusters in the data appear as noise in the density-biased and blue-noise samples, while VAS fails to capture any trends.

data. Approaches like VAS [75] targeted similar goals, but the VAS objectives ultimately optimize for coverage rather than attempt to model human perception directly. Prior work used perceptual models in approximate query processing (AQP) for height estimation in bar charts [6] but existing literature lacks sampling algorithms that directly optimize for visual perception in scatterplots.

In this paper, we present a novel sampling method—*perception-aware sampling*—that uses a model of human perception to derive samples that more effectively represent information in 2-dimensional scatterplot visualizations. Our work relies on four key insights:

- *Saliency maps can serve as a close proxy of perception.* While prior work recognized the importance of “visualization-awareness” in sampling, existing objectives focused on coverage (represent as much of the shape of the underlying data as possible), rather than measures of how a human user would perceive the visualization [75]. We argue that we need not only visualization-awareness but also *perception-awareness*. Luckily, a tool that *implicitly* emulates human perception exists. We propose to employ established *saliency models*, commonly used in computer vision, that predict areas of a visualization that attract viewers’ attention [67]. These models produce *saliency maps*—essentially heatmaps—predicting eye-gaze locations in human interactions with a visualization [18, 19, 48, 67, 96]. We augment saliency with density information—a crucial element in how humans perceive a visualization [107]—to design a more robust perceptual model.
- *A good sample distorts saliency as little as possible.* Intuitively, highly-salient areas are important in a visualization, as human focus is drawn to these areas. If the saliency of a sample differs from the saliency of the original data, this indicates that a human *perceives* this sample differently, as their focus is drawn towards different areas. Our key insight is that the saliency map of the sample should match the saliency map of the original data as much as possible. Intuitively, smaller difference between the two maps corresponds to smaller perceptual distortion in the sample.
- *To preserve saliency, we also need to account for coverage.* The saliency of an area can be impacted by data in surrounding areas. For example, outliers in a visualization often draw attention and thus have high saliency; but a sample with only the outlier points will no longer demonstrate the same saliency (as these points would no longer be perceived as outliers). Therefore, to achieve high perceptual quality in the resulting sample, the sampling strategy needs to incorporate saliency with coverage to preserve the general data shape.
- *Limitations in human perception allow for visual approximations.* In visual data exploration, analysts typically look for patterns, trends, and other insights, but they do not typically look at visualizations

¹Small values of r (prioritizing dense areas) improve runtimes, but worsen coverage; e.g., for $r = 0$ blue-noise acts like random.

to *read* individual data points. Moreover, humans become less sensitive to small value perturbations in a complex visualization, which means that we can allow inaccuracies in the presented data, as long as the visualization preserves the overall trends [44]. We exploit these factors to produce a compressed representation of the data and generate *approximate visualizations*.

We provide an overview of our approach, including more discussion on these intuitions and design choices, in Section 2.

Contributions and outline. To the best of our knowledge, our work is the first to explicitly model perception as an objective in sampling for scatterplot visualizations. We organize our contributions as follows.

- We provide an overview of our sampling methodology, discuss important background literature, and formally define the problem of perception-aware sampling for scatterplots. [Section 2]
- We propose *perception-augmented databases* and design PAwS, a hybrid method based on Max-Min diverse sampling that employs perception weights through a distance re-scaling mechanism. [Section 3]
- We introduce APPROPAwS, a strategy that generates approximate visualizations, through a novel perception-aware compressed representation of the data. The key idea is to fragment the visual canvas into rectangular regions of similar perceptual significance, and we compress the data by adjusting the area size and data density each region encompassed. Then, we use a modified PAwS sampling that selects boxes to sample from and draws points uniformly at random within a box. [Section 4]
- Measuring the quality of a sample is non-trivial, especially for the novel objective of perception-awareness. We contribute a detailed discussion on five metrics we use to evaluate the quality of the sampling algorithms, including an established image similarity metric that measures the difference between two visualizations in the saliency dimension. We discuss additional metrics and their implications. [Section 5]
- We present an extensive evaluation of our methods against five state-of-the-art sampling algorithms, over six datasets with diverse underlying trends and sizes. We demonstrate that our sampling strategies have robust performance over the five metrics, and consistently outperform the alternatives. We observe that PAwS has emphasized benefits at smaller sampling rates, and scales better than the state-of-the-art. Further, we show that APPROPAwS achieves high-quality approximate visualizations at various levels of compression, with results comparable to PAwS, but up to 100x faster for large datasets. A user study further supports our findings and confirms PAwS samples are frequently preferred by humans. [Section 6]

2 Perception-Aware Sampling: Overview and Background

In this section, we present an overview of our approach, along with intuitions and necessary background. We start by describing our insights on modeling perception, and how to measure the perceptual quality of a sample. We proceed to formally define the problem of perception-aware sampling. We then discuss the intuitions driving the design of our perception-aware sampling algorithm. We pursue

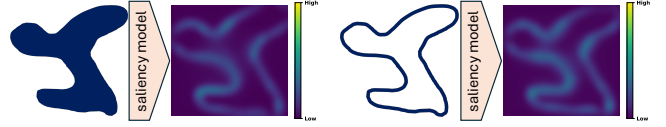


Figure 3: Human attention focuses on the outline of highly-dense areas. As a result, the saliency maps of the two shapes above—one solid and one hollow—are remarkably similar; yet, the shapes are perceptually different. Our perceptual model avoids this pitfall by augmenting saliency with density information.

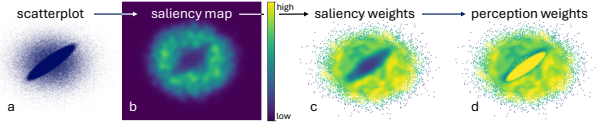


Figure 4: The DVS model [67, 96] derives a saliency map (b) of a scatterplot visualization (a). High saliency identifies areas that are likely to draw human focus. Human attention typically does not focus on the interior of dense areas, so the center of the map has low saliency. This heatmap can be projected on the data to assign *saliency weights* (c). Perception weights (d) augment saliency with density to indicate high perceptual significance for areas that are highly salient or highly dense.

further speed-ups through approximate visualizations based on a perception-aware compression strategy.

2.1 Modeling perception through saliency

Efforts in human perception research have leveraged eye-tracking technologies to model how people perceive images in fields such as computer vision [94, 95] and natural language processing [16, 24]. Such technologies, however, are complex, not as readily available, and hard to incorporate into a sampling workflow.

We propose a new perceptual model based on *saliency models*, commonly used in computer vision, that *predict* areas of a visualization that attract viewers' attention [67]. Saliency models take as input a visualization, and produce *saliency maps*—essentially heatmaps—predicting eye-gaze locations in human interactions with a visualization [18, 19, 48, 67, 96]. Various computer vision tasks have successfully leveraged saliency models: from automatically learning how to zoom in image classification tasks to designing data augmentation techniques for deep learning models [60, 89]. In this paper, we use saliency (augmented with density information) to direct sampling, so that the resulting sample preserves the attention points that saliency maps identify on the original data.

Saliency. Given a saliency model \mathcal{M} and a target visualization V of $m \times n$ pixels, a saliency map $\mathcal{M}(V) : V^{m \times n} \rightarrow [0, 1]^{m \times n}$ is defined as a mapping function from the pixel space to continuous values within the $[0, 1]$ range, i.e., higher values indicate more *salient* pixels. In our implementation, we use an established, state-of-the-art saliency model for visualizations: Data Visualization Saliency (DVS) [67, 96]. Other saliency or perceptual models can be considered in alternative implementations, as this is a black-box component in our framework. Figure 4b shows the saliency map produced by the DVS model over the data in Figure 4a.

Accounting for high-density areas. Saliency models are designed to represent human attention, which is an intuitive proxy for perception, with a one caveat: human focus is drawn on the perimeter of highly-dense elements, ignoring their interior. As a result, the saliency of a solid object is hardly indistinguishable from that of a hollow object (Figure 3); yet, most would agree that these shapes are perceived differently. Thus, we augment saliency models with density information, implementing the following intuition: *an area of high saliency or high density should have a high perceptual value.*

To estimate density, we employ non-parametric kernel density estimators [76, 93, 98]. More formally, given a d -dimensional dataset \mathcal{D} consisting of n points and a density estimation model \mathcal{F} , the estimator $\mathcal{F}(\mathcal{D}) : \mathbb{R}^{n \times d} \rightarrow \mathbb{R}^n$ computes a density estimate for each point in \mathcal{D} . Figure 4d shows the heatmap of *perception weights* computed over the data of Figure 4a; these combine the saliency weights (Figure 4c) with density information. We discuss the details of our approach in Section 3.

Measuring quality. There are no established measures for evaluating the quality of a sample, and in our case quality is based on a novel objective: perception-awareness. Intuitively, a good sample should draw human attention to the same salient areas as if the person was viewing the original dataset. Thus, the saliency map of the sample, should closely resemble the saliency map of the original data. We use *Structural Similarity Index Measure (SSIM)* [102], a well-established metric for comparing images, as our primary measure: given the saliency map of the visualization of a sample and the saliency map over the original data, the SSIM score should be high.

Perception-aware sampling. We are now ready to provide a formal definition of the problem of perception-aware sampling:

DEFINITION 1 (PERCEPTION-AWARE SAMPLING). *Given a dataset \mathcal{D} , a target visualization V , a saliency model \mathcal{M} , an integer $k < |\mathcal{D}|$, and an image-based perceptual similarity function f we want to find $\mathcal{D}' \subset \mathcal{D}$, such that $|\mathcal{D}'| = k$ and $f(\mathcal{M}(V_{\mathcal{D}}), \mathcal{M}(V_{\mathcal{D}'}))$ is maximized, where $V_{\mathcal{D}}$ and $V_{\mathcal{D}'}$ are the visualizations of \mathcal{D} and \mathcal{D}' , respectively, over the target visualization.*

2.2 Perception-aware sampling algorithm

Definition 1 seeks the sample of size k that results in the most similar saliency map as that of the original data. However, since the saliency model and the SSIM measure (which is our perceptual similarity function) are blackbox components, the objective cannot be optimized directly. Iterative approaches may be possible, but the computational cost of the saliency model makes repeated calls to it impractical. Thus, we need to pursue heuristic methods for emulating the desired behavior.

The naive approach of using perception weights as sampling probabilities performs poorly. Intuitively, the reason is that the saliency of an area can be impacted by data in surrounding areas. Consider for example that outliers may draw human attention, but if the sample only contained outlier points, they would no longer be perceived as outliers and the attention patterns could change. Figure 5b shows a sample drawn from the data of Example 1, by using perception weights alone as sampling probabilities. We note that the result resembles uniform random sampling, and similarly fails to capture the small clusters. Based on this intuition, regardless of the perceptual model, perception weights cannot be used in

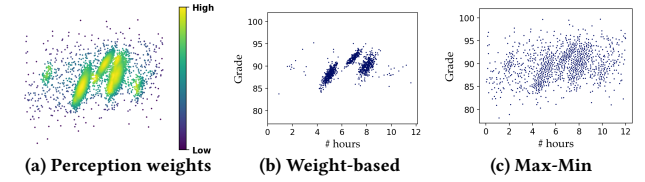


Figure 5: Perception weights for the dataset in Figure 1a. (b) A weight-based sample, which selects points with probabilities proportional to their perception weights, obscures the outlier trend and the two smaller clusters. (c) Max-Min provides uniform data coverage but fails to reveal clusters and trends in the data that become apparent in the saliency map.

a straightforward way to achieve perception-awareness. Our key insight is that, to avoid perceptual distortion in the sample, we need to prioritize areas of high perceptual significance, *and* provide good coverage of the overall data distribution. To achieve coverage, we turn to diverse data selection methods.

Max-Min diversification. Diversity and coverage are related objectives in data selection, and are well-studied by prior work [1, 4, 17, 31, 72]. The goal of data diversification is to select a sample such that the diversity across the selected points is maximized. Prior work has introduced a variety of diversification models; we focus on Max-Min, which is one of the most well-established and frequently-used models [31].

Max-Min diversification, also known as *farthest point* sampling in the visualization and computer vision communities [35, 62, 84], selects points that are *uniformly* dispersed across the data space, and thus provides coverage and preserves the original data shape [32, 72, 101]. Similar to VAS, which also employs a coverage-based loss function, Max-Min sampling is susceptible to noise. However, Max-Min produces a better sample than VAS on the data of Example 1 (Figure 5c) and is also computationally more efficient. The objective of Max-Min is to maximize the diversity of a sample, defined as the minimum pairwise distance of the selected points.

Perception-aware sampling. For Max-Min diversification, there exists a simple approximation algorithm, GMM, that relies on the *farthest-first* traversal heuristic [88]. GMM starts with a random point and keeps selecting the point whose minimum distance to previously selected points is maximized. We design a hybrid method based on the GMM algorithm that employs perception weights through a distance re-scaling mechanism. Our perception-aware sampling algorithm, PAwS, inherits the simplicity and intuition of Max-Min sampling, but re-scales the pairwise similarity scores of data points using the perception weights. This way, it achieves a good balance between coverage and prioritizing the selection of points in areas of high perceptual significance, organically adapting to different data settings. We describe PAwS in Section 3.

2.3 Approximate visualizations

In visual data exploration, analysts typically look for patterns, trends, and other insights, but they do not typically look at visualizations to *read* individual data points. In scatterplots in particular, humans are unlikely to be able to visually perceive small value perturbations in the data, which means that we can allow inaccuracies in the presented data, as long as the visualization preserves the overall trends [44]. Our key insight is that we can generate an

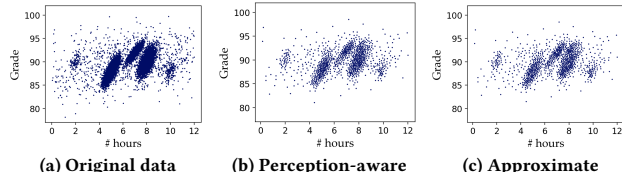


Figure 6: A human user is unlikely to detect that the approximate visualization (c), powered by our perception-aware compression, is automatically constructed and does not sample the underlying data (a). Our perception-aware sampling algorithm generates an actual sample (b), with similar properties as the approximate visualization.

approximate visualization, that does not access or sample the real data at all. We achieve this through a novel perception-aware compression scheme, which works by fragmenting the visual canvas into rectangular regions with similar perception weights; considerations of area size and data density allow for adjusting the level of compression. A modified PAwS sampling selects boxes to sample from, and then draws points uniformly at random within a box.

Figure 6c demonstrates the approximate visualization generated by our APPROPAwS strategy. It displays the same number of points as our PAwS sample (Figure 6b), but these points were not drawn from the original data, but rather, they were “constructed” through our perception-aware compression scheme. Yet, a human would be extremely unlikely to recognize that this is not an actual sample from the original data (Figure 6a). Our APPROPAwS strategy closely emulates the behavior of PAwS, but because it works on the compressed representation and does not access the data directly, it can result in significant runtime gains in large datasets. We discuss the details of this method in Section 4.

2.4 Scope and practical considerations

Our goal in this paper is to establish that objectives targeting human perception (modeled via saliency) achieve more effective data samples compared to state-of-the-art methods. We provide proof-of-concept implementation and demonstrate the effectiveness of perception-aware sampling through extensive quantitative experiments and a user study (Section 6). It is *not* our goal to evaluate how well state-of-the-art saliency models capture visual attention. This has already been established in prior work [18, 19, 48, 67, 96], and we use these state-of-the-art tools as blackboxes.

Saliency maps can be precomputed across specified pairwise combinations of data attributes; these could be determined by historical analyses, domain requirements, and feature selection techniques. The overhead of computing and storing saliency maps only depends on image resolution, **and does not increase with the size of the data**—e.g., for a 1084x924 image, the storage overhead is 438KB and the computational cost is 42 seconds, regardless of data size. This overhead does not impact the running time of our algorithms.

Conceptually, saliency maps are abstract “sketches” of the underlying data, its shape, and trends. Similar to sketching techniques for deriving synopses of data [26], saliency maps form synopses of *the looks* of a dataset. While it may be tempting to consider storing visualizations of the original data as images, this does not address the limitations on the amount of data a user can process nor overplotting, to which saliency models are more robust. Moreover, such images would be static, but data analysts rely on interactive

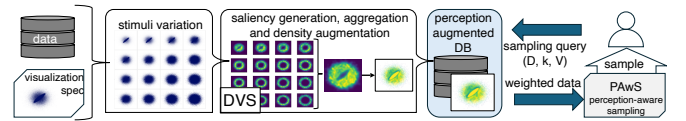


Figure 7: Our perception-augmented DB stores an aggregate saliency heatmap, generated from varied target visualization stimuli, and augmented with density information. Given a sampling query for a target visualization, the perception-augmented DB generates a weighting scheme for the underlying data and uses PAwS (Algorithm 1) to produce a perception-aware sample of the specified size.

visual exploration that allows for filtering, brushing, linking, or zooming operations, and sampling is a fundamental approach in the literature for designing such interactive visualization systems [57].

There are interesting challenges in optimizing the overhead of storing saliency for multiple candidate visualizations, which are called scatterplot matrices (SPLOMs) in the visualization literature [47]. Future work could leverage insights from the computer vision literature—such as saliency mix-up techniques [53], which blend salient regions across multiple images—as a potential direction for synthesizing saliency information across multiple views.

3 Perception Support and Sampling

In this section, we present our primary perception-aware sampling mechanism; Figure 7 provides a visual overview. The *perception-augmented database* augments the original data with saliency information for the target visualizations as meta data. At the time of sampling requests, the perception-augmented DB generates appropriate perception weights and deploys our perception-aware sampling algorithm (PAwS) to derive a sample of the requested size. We proceed to describe how we construct the perception-augmented DB and then present our sampling mechanism.

3.1 Perception-augmented database

Our perception-aware sampling mechanism is built on top of a novel *perception-augmented database*. We construct this perception-augmented database by precomputing and storing a perceptual model of the data for the given target visualizations.

As we described in Section 2, our perception model is built over saliency maps. However, producing a suitable saliency map is more than simply invoking a saliency model. Human perception, and by extension saliency, is affected by the visual features of a visualization (e.g., point size, opacity, canvas aspect ratio) [57, 69]. In Figure 8a, we render the same dataset with varying configurations for the point size (2–16) and opacity (0.1–1), with an aspect ratio of 1.25:1. Figure 8b shows the saliency map that corresponds to each rendering. We observe that for small point sizes and opacity, the visualization highlights areas of higher population density, and the corresponding saliency maps identify these areas as more salient. For large point sizes and opacity, more areas of the visualization appear dense, and the attention focus tends to shift towards the outskirts and outliers.

Selecting a *good* configuration for a scatterplot is non-trivial and it is an active problem in visualization research [57, 69, 84, 85]. Our observations in Figure 8 further demonstrate that different configurations emphasize different aspects of the data. To better preserve these aspects, we follow a stimuli-driven approach to generate

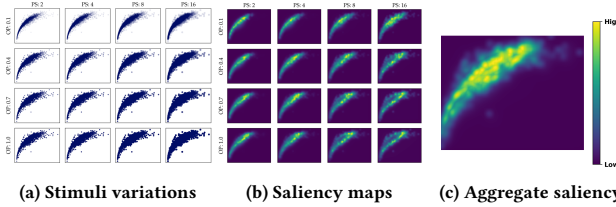


Figure 8: Visual features affect visualizations and saliency. (a) Data visualizations for different point sizes and opacity configurations. (b) Saliency maps produced for each data visualization. (c) Aggregate saliency over the maps in (b).

saliency maps across different configurations and then aggregate them into a single heatmap (Figure 8c). Different aggregation options are possible; in our implementation, we use the maximum saliency value of each pixel across all configurations, as we found it to be more robust and better at preserving different data trends.

Deriving perception weights. The perception-augmented database translates the aggregate saliency map into saliency weights. The saliency map is a 2D matrix assigning saliency values to pixels, which are projected onto data points in the visualization to derive saliency weights (Figure 4). The database stores aggregate saliency maps with a small storage overhead, and saliency weights are computed on the fly with negligible impact on runtime performance.² To derive perception weights (Section 2), we augment saliency with density. We estimate density using non-parametric kernel density estimators [76, 93, 98], assigning higher density weights to points in highly dense areas. Then, for a data point p , with a saliency weight q_1 and a density weight q_2 , the perception weight is equal to $w_p = \max(q_1, \gamma \cdot q_2)$, where $\gamma \in [0, 1]$ balances the influence of density.

Density weights are stored as an additional data attribute, while perception weights are computed on the fly. Using the maximum operator ensures that points are prioritized while sampling if located in highly salient or highly dense areas. To adaptively set γ , we measure the variance of the density weights: when variance is low, density adds little information as all areas have similar density (γ approaches zero); when variance is high, density plays a larger role. In our experiments, we map the density variance of a dataset into a sigmoid function to obtain a $\gamma \in [0, 1]$, assigning γ values closer to one for datasets with larger density variance. Figure 4 shows an example of deriving perception weights.

3.2 Perception-aware data selection

Users can query the perception-augmented DB to retrieve a sample of the desired size for their target visualization. The perception-aware DB invokes PAwS (Algorithm 1) on the dataset \mathcal{D} of size n , with target visualization V and desired sample size $k < |\mathcal{D}|$. We assume a metric distance function $d : \mathcal{D} \times \mathcal{D} \rightarrow \mathbb{R}_0^+$ representing the pairwise similarities of points over the two visualization attributes and a set of perception weights $\mathcal{W} = \{w_{p_1}, w_{p_2}, \dots, w_{p_n}\}$ that the DB computes on the fly.

Our goal is to select a sample $\mathcal{D}' \subseteq \mathcal{D}$ of size k that maximizes the *perceptual* similarity of \mathcal{D}' to the original dataset \mathcal{D} ,

²Saliency weights could be stored in the perception-augmented database, but while storage overhead per point is constant, the total storage overhead would grow with the size of the data.

Algorithm 1 PAwS (Perception-Aware Sampling)

```

Input:  $\mathcal{D}$ : Dataset of  $n$  point
 $\mathcal{W} = \{w_p : p \in \mathcal{D}\}$ : Perception weights of points in  $\mathcal{D}$ 
 $k \in \mathbb{Z}^+$ 
Output:  $\mathcal{D}' \subseteq \mathcal{D}$  of size  $k$ 
1: procedure PAwS( $\mathcal{D}, \mathcal{W}, k$ )
2:    $\mathcal{D}' \leftarrow$  a randomly chosen point in  $\mathcal{D}$ 
3:   while  $|\mathcal{D}'| < k$  do
4:      $p^* \leftarrow \operatorname{argmax}_{y \in \mathcal{D}} w_y \cdot \min_{x \in \mathcal{D}'} d(y, x)$ 
5:      $\mathcal{D}' \leftarrow \mathcal{D}' \cup \{p^*\}$ 
return  $\mathcal{D}'$ 

```

i.e., the similarity of the saliency maps of \mathcal{D}' and \mathcal{D} should be maximized. Given the blackbox nature of saliency models, PAwS follows a heuristic approach that balances coverage objectives with prioritizing the selection of points with high perception weights.

PAwS adapts the greedy selection strategy in Max-Min sampling: It initially selects a random point, and proceeds to augment the sample \mathcal{D}' greedily, by adding the point p^* with the maximum score $s_{p^*} = w_{p^*} \cdot \min_{x \in \mathcal{D}'} d(p^*, x)$. This score is defined as the product of the distance of the point to the existing sample and its perception weight. Thus, the objective penalizes points that have low perception weights, as well as points that are too close to the existing sample. This strategy is analogous to data augmentation techniques in computer vision that balance saliency and coverage [60].

Running time. Algorithm 1 has $O(kn)$ running time, if the implementation maintains the pairwise distances of each point to the sample ($\min_{x \in \mathcal{D}'} d(y, x)$ in line 4) by only computing distances to each newly added point. Similar implementations have been used in the literature [56, 101].

4 Approximate Visualizations

Sampling operations should be fast, to avoid hindering visual analytics workflows. While PAwS is faster than several state-of-the-art approaches (as we will see in Section 6), further boosting efficiency and scaling is desirable. In this section, we discuss an extension to the functionality of the perception-augmented database that allows for several orders of magnitude speed-up in sampling times on large datasets. Our approach relies on a fundamental limitation in human perception: humans are typically unable to perceive small perturbations in visualized data (recall the example of Figure 6). This means that, as long as our perception goals are met, we do not need accurate data values in the sample.

Figure 9 demonstrates the high-level workflow of our *approximate visualization* module. The perception-augmented DB uses a quad-tree partitioning scheme to produce a compressed representation of the data based on the perception model. Intuitively, the compressed representation fragments the canvas area into bounding boxes of different sizes, so that the data that falls within each box is somewhat evenly distributed and has similar perception weights. Our adapted sampling algorithm, APPROPAwS (Algorithm 2), generates a set of representative points for each box, drawn uniformly at random within the box area. It then greedily selects a point at a time, based on a combination of perception and coverage objectives (like PAwS), replacing the point with another random one in the same box. APPROPAwS achieves runtime gains simply on the premise of working over a small dataset of randomly-drawn points, so these gains are more pronounced the larger the original data is.

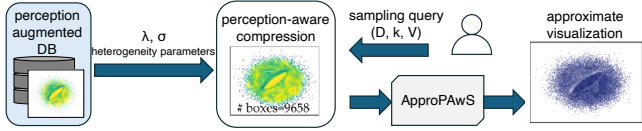


Figure 9: The perception-augmented DB can store a compressed representation of the data using a quad-tree partitioning structure. Each cell conforms to uniformity requirements for the data distribution and perception weights, which control the compression level. APPROPAwS (Algorithm 2) can then generate a sample directly from the perception-aware compression, resulting in an approximate visualization.

4.1 Perception-aware compression

We create a compressed representation of the dataset \mathcal{D} over the two dimensions relevant to the target visualization. Our compression mechanism splits the visualization canvas in a quad-tree hierarchical partitioning fashion: any cell that fails to meet certain data distribution or perception homogeneity requirements is split into four smaller cells. The partitioning terminates with a collection of non-overlapping bounding boxes of different sizes, such that each box (1) approximates well the distribution of data within that box, and (2) covers areas with roughly similar perception weights. We explain these criteria below.

Data approximation. Our goal is to use the compressed representation to draw samples uniformly at random within each box, instead of accessing the data itself. Therefore, this stopping criterion ensures that indeed, a sample drawn uniformly at random from the box is close enough to the true data points of the box. We use the *Chamfer* (pseudo)-distance (CD) as our metric. CD is a commonly used metric in the computer vision literature for designing generative neural network models for reconstructing 3D point clouds [3, 37, 104]. It compares the similarity of two unordered sets of points $\mathcal{S}_1, \mathcal{S}_2$ and is defined as follows:

$$d_{CD}(\mathcal{S}_1, \mathcal{S}_2) = \frac{1}{2} \left(\frac{1}{|\mathcal{S}_1|} \sum_{x \in \mathcal{S}_1} \min_{y \in \mathcal{S}_2} \|x - y\|_2 + \frac{1}{|\mathcal{S}_2|} \sum_{y \in \mathcal{S}_2} \min_{x \in \mathcal{S}_1} \|x - y\|_2 \right)$$

The Chamfer distance measures how close every point in the actual data \mathcal{S}_1 is to their nearest neighbor in the random sample \mathcal{S}_2 , and vice versa, and computes the average. A box is split if d_{CD} is above a preset threshold λ .

Homogeneity of perception weights. Since we generate points randomly within each box, we need the true data within the box to have similar perception weights. We split a box if the variance of the perception weights of the data within the box is higher than a preset threshold σ .

Figure 10a shows a visual representation of the compression of a dataset for varied values of λ and σ . These thresholds affect the number of boxes in the final compression. Intuitively, more boxes result in lower compression and lower distortion of the final visualization. In this case, we see the lowest compression in the upper left corner and the highest compression in the lowest right corner of Figure 10a. Figure 10b shows the corresponding approximate visualizations for each compression (produced by our APPROPAwS, discussed next). We note that even at the lowest compression (most boxes), the size of the representation is only 1.2 MB; the resulting visualization achieves perceptual similarity on par with PAwS, with a runtime that is about 100x faster (Section 6.2).

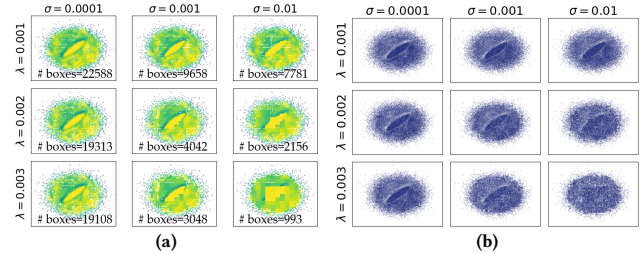


Figure 10: Varying the thresholds λ and σ results in different compression rates (a). Lower compression rates (lower values for λ and σ) lead to lower distortion in the approximate visualizations by APPROPAwS (b), shown for a sample size of $k = 9,611$ points.

Algorithm 2 APPROPAwS (Approximate PAwS)

```

Input:  $\mathcal{P}$ : partitions in the compressed representation of  $\mathcal{D}$ 
 $\mathcal{W}_{\mathcal{P}} = \{w_b : b \in \mathcal{P}\}$ : Perception weights of boxes in  $\mathcal{P}$ 
 $k \in \mathbb{Z}^+$ 
Output:  $\mathcal{D}'$  of size  $k$ 
1: procedure APPROPAwS( $\mathcal{P}, \mathcal{W}_{\mathcal{P}}, k$ )
2:    $R \leftarrow \emptyset$  ▷ Construct a set of representatives with  $C$  random points from each box
3:   for  $\forall b \in \mathcal{P}$  do
4:      $\mathcal{R}_b \leftarrow C$  random points in  $b$ ,  $\forall r \in \mathcal{R}_b, r.w = w_b$  ▷ Initialize the sample with a random point
5:      $R \leftarrow R \cup \mathcal{R}_b$ 
6:    $\mathcal{D}' \leftarrow \text{random point in } \mathcal{P}$  ▷ Initialize the sample with a random point
7:   while  $|\mathcal{D}'| < k$  do
8:      $v \leftarrow \operatorname{argmax}_{r \in R} r.w \cdot \min_{x \in \mathcal{D}'} d(r, x)$  ▷ Replace  $v$  in  $\mathcal{R}$ 
9:      $\mathcal{D}' \leftarrow \mathcal{D}' \cup \{v\}$ 
10:     $r' \leftarrow \text{random point from } b \in \mathcal{P}, \text{ where } v \in b$ 
11:     $R \leftarrow (R \setminus v) \cup r'$ 
return  $\mathcal{D}'$ 

```

4.2 Approximate PAwS

Given a perception-aware compression, our APPROPAwS algorithm (Algorithm 2) generates a sample with points drawn from the compressed representation, rather than from the actual data. Intuitively, APPROPAwS generates and maintains a small representative dataset \mathcal{R} on the fly, and selects points greedily from \mathcal{R} using the same combined perception and coverage objective as PAwS. The algorithm initializes \mathcal{R} by generating uniformly at random a small, constant number C of points from every box in the compressed representation (lines 3–5). Using $C > 1$ makes the algorithm robust to poor random draws (e.g., a box never getting picked due to a poor representative). When a point is selected for the sample, it gets a replacement from the same box in the representative set (line 11). Even though APPROPAwS does not access the actual data, the construction of the compressed representation ensures that the random points drawn from the boxes conform to the data distribution and perception levels of the original data.

Running Time. The running time of APPROPAwS is $O(k^2 + kC|\mathcal{P}|)$, where C is the number of points we draw from each box, and $|\mathcal{P}|$ is the number of boxes in the compression. When we replace a representative, we need to compute the distance of the new point to the current sample ($O(k^2)$ factor). The second term is similar to that of PAwS, but note that $C \cdot |\mathcal{P}| \ll n$, when C is a small constant and $|\mathcal{P}| \ll n$. This means that APPROPAwS leads to more gains for large datasets, but when n is small the runtime may actually be worse than PAwS due to the additional factors.

Metric	Metric Type	Range	Normalization
SSIM (\uparrow)	image-based	[-1, 1]	–
CC (\uparrow)	distribution-based	[-1, 1]	by variance
SIM (\uparrow)	distribution-based	[0, 1]	by sum
JSD (\downarrow)	distribution-based	[0, 1]	by sum
EMD (\downarrow)	distribution-based	unbounded	by sum

Figure 11: We use several metrics to evaluate the *perceptual similarity* of samples to the original data. The top three metrics measure similarity, and the last two dissimilarity. We report $1 - JSD$ in our experiments, which is a similarity metric.

5 Perceptual Similarity Metrics

In this work, we posit that a sample should not distort the attention focus areas of the original data and express *perceptual similarity* as the similarity between their saliency maps. This insight allows us to use well-established image-based and distribution-based similarity metrics, which we introduce below.

Metrics for perceptual similarity. Saliency maps are stored and visualized as images; thus, we use a well-established image-based metric as our primary metric: Structural Similarity Index Measure (SSIM) [102]. We further evaluate four distribution-based metrics from the saliency literature [18]. These metrics treat a saliency map as a distribution over pixels and measure how accurately a saliency model predicts the attention focus areas of a dataset.

Structural Similarity Index Measure (SSIM) [image-based] is a well-known image similarity metric, frequently used as a loss function in computer vision problems [59, 109]. The metric assumes two images split into fixed-size windows. The SSIM score is computed as the mean of similarity scores across windows measured over luminance (ℓ), contrast (c), and structure (s), i.e., $SSIM(\theta_1, \theta_2) = \ell(\theta_1, \theta_2)^\alpha \cdot c(\theta_1, \theta_2)^\beta \cdot s(\theta_1, \theta_2)^\gamma$. If $\alpha = \beta = \gamma = 1$, all three terms affect the score equally, while each term in the product depends on statistical information like the mean pixel value and variance of pixel values of an image window.

Pearson’s Correlation Coefficient (CC) [distribution-based] measures linear correlation across two random variables. We standardize the saliency maps $\mathcal{M}(V_{\mathcal{D}'})$ and $\mathcal{M}(V_{\mathcal{D}})$ and measure their correlation as:

$$CC(\mathcal{M}(V_{\mathcal{D}'}), \mathcal{M}(V_{\mathcal{D}})) = \frac{COV(\mathcal{M}(V_{\mathcal{D}'}), \mathcal{M}(V_{\mathcal{D}}))}{\sigma(\mathcal{M}(V_{\mathcal{D}})) \cdot \sigma(\mathcal{M}(V_{\mathcal{D}}))}$$

CC takes values in the $[-1, 1]$ range where higher values indicate higher correlation (higher similarity). A value of 0 indicates no correlation (low similarity).

Similarity (SIM) [distribution-based] measures the similarity of two distributions by computing a histogram intersection. We normalize the saliency maps to derive the distributions $p_{\mathcal{D}'}$ and $q_{\mathcal{D}}$ over I pixels, and compute SIM as follows:

$$SIM(p_{\mathcal{D}'}, q_{\mathcal{D}}) = \sum_{i \in [I]} \min(p_{\mathcal{D}'}(i), q_{\mathcal{D}}(i))$$

For every pixel of the saliency maps, we take the minimum probability value between the sample and the dataset distribution. SIM takes values in the $[0, 1]$ range: a value equal to 1 indicates a perfect distribution match, and 0 no match at all.

Jensen-Shannon Divergence (JSD) [distribution-based] measures *dissimilarity* among two probability distributions. We normalize the saliency maps to derive the distributions $p_{\mathcal{D}'}$ and $q_{\mathcal{D}}$ and compute JSD as:

$$JSD(p_{\mathcal{D}'}, q_{\mathcal{D}}) = \frac{1}{2} D_{KL}(p_{\mathcal{D}'} || \mu) + \frac{1}{2} D_{KL}(q_{\mathcal{D}} || \mu)$$

where μ is the point-wise mean of $p_{\mathcal{D}'}$ and $q_{\mathcal{D}}$. D_{KL} is the KL-divergence, defined as:

$$D_{KL}(p_{\mathcal{D}'} || \mu) = \sum_{i \in [I]} p_{\mathcal{D}'}(i) \log \left(\frac{p_{\mathcal{D}'}(i)}{\mu(i)} \right)$$

JSD is a symmetric version of KL-divergence and takes values in the $[0, 1]$ range. Lower values indicate higher similarity: e.g., the JSD of two identical distributions is equal to zero.

Earth Mover’s Distance (EMD) [distribution-based] measures the spatial dissimilarity across two distributions over a metric space. The distributions $p_{\mathcal{D}'}$ and $q_{\mathcal{D}}$ are two-dimensional histograms with a number of bins equal to the resolution of the saliency maps. Given a function that models the pairwise cost of *moving* a unit of probability mass from one bin to another, EMD is equal to the minimum cost of transforming one distribution into the other, and is computed by solving an optimal transportation problem [18, 78, 79]. Computing EMD involves solving a linear program, which can be impractical to compute for large image sizes. Thus, we follow the methodology of Bylinskii et al. [18], and reduce the size of the saliency images to $\sim 1/32$ of their original resolution. We use an open-source library for the implementation,³ and highlight that, even for reduced image sizes, EMD is computationally expensive.

Discussion. We use well-established distribution and image-based metrics for measuring the similarity across two saliency maps. Interpreting their behavior and the mechanism based on which they penalize mismatches across saliency maps is a separate research area and is not straightforward [18, 73]. As an example, Bylinskii et al. [18] find CC is affected symmetrically by false positives and negatives, i.e., indicating an area is salient when it is not and vice versa, while SIM is mostly affected by false negatives. We refer the reader to the in-depth experimental evaluation across different metrics by Bylinskii et al. [18] for a better understanding of their behavior, and guidelines on how to use them in practice.

A separate research question is how well these metrics align with human perception [61]. For instance, despite popular belief that SSIM is a perceptual-based similarity metric for images, there have been known cases in the literature where human judgment does not align well with the SSIM score [73]. Thus, designing better metrics for image similarity is still an active research problem [108]. **It is not the focus of this work to contribute better and more robust similarity metrics; we lean on the state-of-the-art and use a variety of metrics to guide our evaluation.**

6 Experimental Evaluation

In this section, we present an extensive evaluation of our perception-aware sampling methods, against five state-of-the-art and baseline approaches, over six datasets with diverse characteristics. Our experiments demonstrate that PAwS robustly outperforms other methods in producing samples that are *perceptually similar* to the

³<https://github.com/wmayner/pyemd>

original data, and achieves desirable levels of perceptual similarity at lower sample sizes. It is also orders of magnitude faster than competing state-of-the-art on large datasets (Section 6.1). Moreover, the approximate visualizations of APPROPAwS using the perception-aware compression achieve similar levels of perceptual similarity to PAwS, with 100x gains in runtime performance on our largest dataset of ~ 3.5 M data points. (Section 6.2).

We proceed to describe our datasets, state-of-the-art sampling algorithms, and baselines. We used Python 3.8 for the code implementation and ran the experiments on one cluster node with a 2.3 GHz 8-Core Intel Core i9 and 16 GB RAM.

Datasets. We collected six datasets with a diversity of patterns, underlying trends, and sizes ranging from 11.5K to 3.5M points. We embed all datasets into a 2D space for the scatterplot visualizations, normalized in the $[0, 1] \times [0, 1]$ range (shown in Figure 12).

MNIST [58] consists of 70,000 images for different handwritten digits and is commonly used in the visualization literature for clustering analysis and perception research [84, 107]. We use a version of the dataset projected onto 2D space using the t-SNE dimensionality reduction method.⁴

Estate Correlation is a dataset of New York real estate pricing⁵, which consists of 17,614 entries and 8 continuous attributes. We selected two moderately correlated attributes for the visualization.

Estate GIS reuses the New York real estate pricing dataset (17,614 entries) with two different visualization attributes resulting in a shape most suitable for outlier detection.

Epileptic Seizure [8] describes EEG information⁶. The dataset has 11,500 entries with 178 attributes. We selected two uncorrelated attributes for the visualization.

ACSI [30] is one of the ACS datasets for research in fair machine learning. It consists of 250,847 entries and 6 continuous attributes. We chose two attributes that visualize into an abacus-like shape with no specific trend.

Hidden Correlation is a synthetic two-dimensional dataset that consists of ~ 3.5 million records. 97.5% of the dataset consists of highly correlated points ($\rho = 0.9$) while 2.5% of non-correlated points ($\rho = 0$). Due to high visual cluster, the correlation trend is often obscured in the visualization. Depending on the sampling methods, the correlated points and uncorrelated points may be sampled at different rates, driving the user to see correlations of varying strengths, thus making this synthesized dataset an ideal test bed for perception-aware sampling methods.

Methods. Our evaluation compares our algorithms (PAwS and APPROPAwS) against five baselines, including probabilistic-based methods (RANDOM and DBS), diversity-based methods (MAX-MIN and VAS), and other state-of-the-art (BLUE-NOISE):

PAwS is our primary algorithm for selecting perception-aware samples using the saliency models stored in a perception-augmented database (Section 3).

APPROPAwS is our approximate visualization method, which generates samples through perception-aware compression (Section 4).

⁴<https://github.com/thu-vis/libssampling/blob/master/data/mnist.npz>

⁵<https://www.kaggle.com/datasets/ivanchvez/ny-rental-properties-pricing>

⁶<https://www.kaggle.com/datasets/harunshimanto/epileptic-seizure-recognition>

RANDOM is standard uniform random sampling, an extremely common method, owing to its simplicity and accessibility [91, 107].

MAX-MIN, also known as Farthest-point sampling [35, 88], selects a sample $\mathcal{D}' \subseteq \mathcal{D}$ of size k that maximizes the minimum distance across the selected points. We use GMM [88], a greedy approximation algorithm ($O(kn)$) that starts with a randomly-selected point and adds the point farthest from the sample at every step.

VAS is a visualization-aware sampling method for scatterplots [75]. It selects a sample $\mathcal{D}' \subseteq \mathcal{D}$ of size k such that for any point $x \in \mathcal{D}$ $\exists y \in \mathcal{D}'$ that is close enough to x . Closeness is controlled through a user-specified parameter ϵ .⁷ VAS uses the Expand + Shrink (ES) local search algorithm, which starts with a candidate solution of k points and keeps swapping a point at a time until no swap offers improvement. Typically, ES converges to a solution in less than half an hour [75]. Park et al. [75] discuss a runtime optimization using R-trees, but only recommend it for sample sizes of more than 10K points. For smaller sizes, the overhead of maintaining the R-tree dominates the running time. In this work, we implement the vanilla version of the ES algorithm and refer to the original paper for analyzing improvements in running time. Similar to MAX-MIN, VAS is effective in preserving data shape and maximizing coverage.

DBS probabilistically over-samples points in sparse areas and under-samples points in denser areas to preserve relative density information [74]. We use the open-source implementation of Yuan et al. [107]⁸, which employs a KNN neighbors algorithm and samples a point with a probability proportional to its K-farthest neighbor distance. Intuitively, if this distance value is high then the point lies in a sparse area and thus has a higher probability of being selected.

BLUE-NOISE sampling selects a set of points that are at least some radius r far apart from each other, for some pre-specified value of r [106]. A common implementation uses the dart-throwing technique [25]: given a sampling radius r , the algorithm randomly selects a point; if the point's distance from the sample is greater than r , then it is added to the sample, and it is rejected otherwise. After a certain number of rejections, the algorithm reduces the value of r to reach the desired sample size. We note that the setting of r affects the algorithm's behavior: the smaller the r , the more the algorithm focuses on prioritizing dense areas. BLUE-NOISE aims for a balanced representation across sparse and dense areas, and thus optimizes for data shape and coverage. We use the open-source implementation of Yuan et al. [107].

Experimental design. Here, we discuss our methodology in creating the perception-augmented DB, computing perceptual similarity, and selecting sample sizes.

Scatterplot rendering and perception weights. As we discussed in Section 3.1, visual features, such as point size and opacity, affect the saliency information in the visualization. The effect can be significant; e.g., in hidden correlation, the correlation trend is only visible for small marker size and low opacity (Figure 12f). Our perception-augmented DBs store *aggregate* saliency maps over visual configurations varying point size (PS: {2px, 4px, 8px, 16px}) and opacity (OP: {10%, 40%, 70%, 100%}), on a fixed canvas size 14 in \times 12 in

⁷Since the data lies in a unit square after normalization, we set $\epsilon = \sqrt{2}/100$ because $\sqrt{2}$ is an upper bound on the diameter value of \mathcal{D} .

⁸<https://github.com/thu-vis/libssampling/blob/master/sampling/SamplingMethods.py>

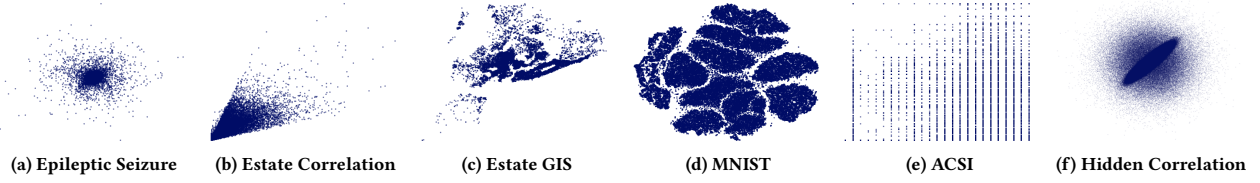


Figure 12: Visualizations of the datasets we use in the experimental evaluation.

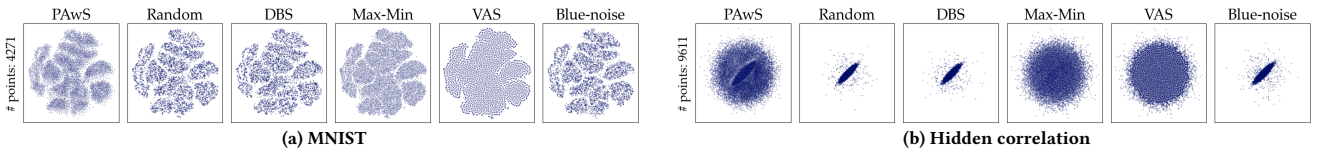


Figure 13: PAwS prioritizes the selection of data points in salient and high-density areas, while providing data coverage. MAX-MIN and VAS optimize for coverage, and may fail to preserve trends (e.g., in hidden correlation). RANDOM and DBS preserve relative density, while BLUE-NOISE aims for a balanced representation among dense and sparse areas, but its behavior varies and sometimes behaves like random sampling.

(i.e., aspect ratio of 1.16 and resolution $1,085 \times 924$). The aggregate saliency maps are projected onto the data to derive saliency weights, which are then augmented with density information. In our implementation, we employ a non-parametric, state-of-the-art, tree-based, density estimator from the scikit-learn library [12, 77].⁹

Perceptual similarity. We express the perceptual similarity of two visualizations as the similarity between their saliencies. Since visual features affect perception and saliency, we use 16 configurations with the point size and opacity settings discussed above to generate saliency maps for the original data and each sample. We compare the saliency similarity of each pair (original and sample) with the same configuration, and compute the final perceptual similarity as the average across all 16 configurations. We report this average score along with a 95% confidence interval across the 16 configurations, and do the same for all five metrics (Section 5).

Sample sizes. We select sample sizes using the Weber-Fechner Law, which states the relationship between change in stimulus and perception is logarithmic [80]—this methodology is favored in the visualization literature. We follow Yuan et al. [107] and experiment with sample sizes $\{250, 375, 844, 1898, 4271, 9611\}$, defined by the geometric series $\{250 \times 1.5^0, 250 \times 1.5^1, 250 \times 1.5^3, 250 \times 1.5^5, 250 \times 1.5^7, 250 \times 1.5^9\}$, where 1.5 is a constant value in the methodology proposed by the authors [107].

6.1 Perceptual quality of sampling methods

In this section, we evaluate perception-aware sampling (PAwS) and the other state-of-the-art methods with respect to their ability to avoid perceptual distortion in the resulting visualizations. We first discuss the behavior of different algorithms, as this is showcased through some qualitative results, and then report on the perceptual similarity scores samples achieve across all metrics. We further evaluate PAwS via a user study, and put results in context with their runtime performance.

Figure 13 showcases samples produced by each method on two of our datasets. Since MAX-MIN and VAS optimize for coverage, they

⁹Off-the-shelf density estimators were not scalable for hidden correlation ($\sim 3.5M$), and we approximated the behavior by rendering the original dat using a small point & opacity configuration (i.e., PS=2px, OP=10%).

select points that are evenly distributed across the data space, and can fail to capture trends at small sample sizes. On the other hand, RANDOM and DBS prioritize areas of density, thus failing to capture the overall shape. BLUE-NOISE achieves better balance by adaptively prioritizing the selection of points in sparse and dense areas, but behaves like random sampling on the hidden correlation dataset. PAwS prioritizes points in areas of high perceptual significance without sacrificing coverage, resulting in samples that represent well the overall shape and trends. In Figure 13b, the PAwS sample identifies the correlation trend, when other methods miss it.

Figure 14 reports quantitative results on the efficacy and efficiency of all algorithms. Due to space limitations, we omit or summarize some results; we refer the interested reader to Appendix A. On the left side of Figure 14, we report on each sampling algorithm’s effectiveness at producing perceptually good samples, using our five metrics. The first row of plots (Estate Correlation) shows the perceptual similarity achieved by all algorithms in samples generated over the Estate Correlation dataset. PAwS achieves high scores across all metrics and sample sizes. The performance of other methods varies a bit across metrics, but generally, MAX-MIN, VAS, and BLUE-NOISE lag in perceptual similarity scores until the sample size gets larger. RANDOM and DBS achieve much worse scores than the other algorithms.

In the second row (All data), we average the perceptual similarity scores for each method across all datasets, to provide a more holistic view of the algorithms’ behavior. The probabilistic methods consistently underperform, with respect to all metrics. The relative performance of MAX-MIN, VAS, and BLUE-NOISE varies across the different metrics, but what remains constant is that PAwS demonstrates superior performance with respect to all metrics. These results also demonstrate that PAwS needs smaller sample sizes to achieve a certain level of perception similarity. E.g., PAwS scores 0.75 SSIM similarity on average for a sample of 844 points, when VAS needs 5x bigger sample.

The third row (SSIM Metric) reports the algorithms’ performance across five datasets (the corresponding plot for the Estate Correlation dataset appears in the first row), focusing on the SSIM metric, which is our only image-based metric. We note that it is normal for sampling behavior to vary across datasets, given the

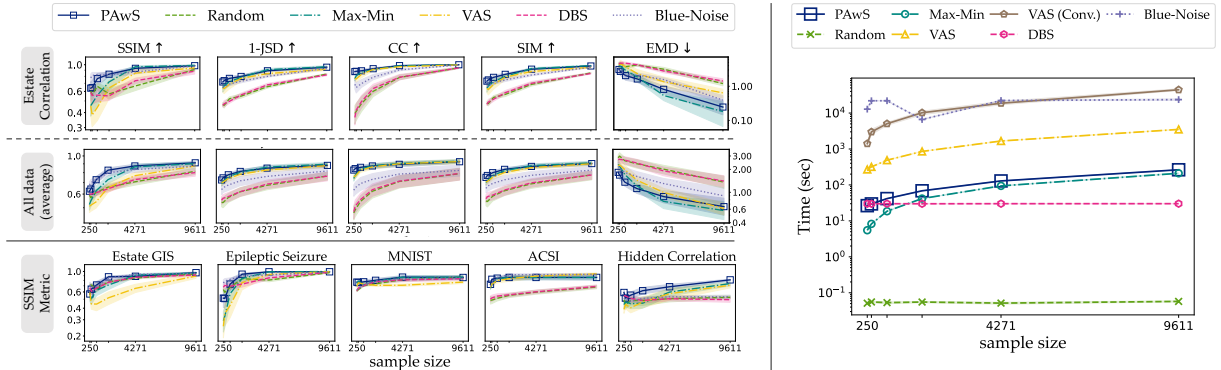


Figure 14: PAwS shows strong performance across all metrics and is also more scalable than other state-of-the-art on hidden correlation, a $\sim 3.5M$ dataset. Only probabilistic-based methods are faster but perform poorly at producing perceptually good samples.

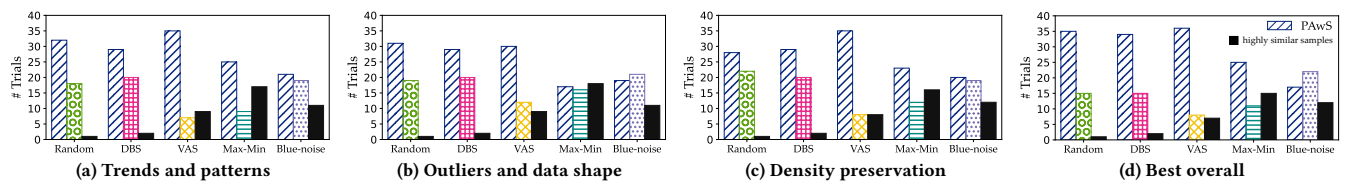


Figure 15: Users' preferences across all datasets for: (a) the sample that better represents correlation trends, clusters, and other patterns, (b) the sample that better represents outliers and overall data shape, (c) the sample that better represents density variations, and (d) the best overall sample. When users could not pick among samples because of high similarity, they could opt for that option.

different shapes and trends, or lack thereof. However, we observe that PAwS robustly achieves high scores across all datasets, and outperforms other methods in most cases. We note that, intuitively, perceptual similarity increases as sample sizes grow for all methods, so differences are often more pronounced at smaller sizes. On the MNIST data, all methods are close in similarity scores; this is due to the clustering structure and even density across data regions, which allows perception-agnostic methods to perform well despite their limitations. In ACSI, the probabilistic methods are distinctly worse, but the others achieve similar results.

User study. To evaluate PAwS, we conducted a user study assessing its efficacy across three key aspects: (1) preserving density variations, (2) retaining outliers and overall data shape, and (3) maintaining correlation trends, clusters, and other patterns.

We recruited 17 Computer Science students (Mean_{age} = 27, SD_{age} = 3.4) familiar with statistical concepts, as verified through a few trivial questions. In each task, participants viewed the full dataset—where they could adjust marker transparency—and compared a PAwS sample against an alternative generated by a state-of-the-art method. For each dataset, they compared five sample pairs across the three evaluation criteria, followed by an overall preference question. We chose sample sizes according to the original dataset sizes: 1,898 ($\sim 16\%$) for Epileptic Seizure, 1,898 ($\sim 11\%$) for Estate Correlation and Estate GIS; 4,571 ($\sim 6\%$) for MNIST; and 9,611 ($\sim 4\%$ and $\sim 0.3\%$) for the larger ACSI and Hidden Correlation datasets. The study included 6 datasets \times 5 sample pairs \times 4 tasks, resulting in 120 tasks. To distribute the workload, each participant completed tasks for 3 of the 6 datasets, and the datasets were evenly presented to participants.

Figure 15 presents aggregated results across all datasets and participants: i.e., ~ 50 trials per sample pair. For each sample pair—comparing a PAwS sample to an alternative sample—we report how

often participants preferred each method across all trials. PAwS shows strong performance across all four evaluation criteria, while BLUE-NOISE is the method ranked closer to it in terms of user preference. However, BLUE-NOISE is computationally expensive and often fails to preserve data shape—most notably on Hidden Correlation—leading participants to favor PAwS there. Probabilistic-based methods generally rank below PAwS, but we observed participants only decisively prefer PAwS when those methods fail to capture shape and outliers (as is the case on Hidden Correlation and ACSI). Finally, while PAwS outperforms diversity-based methods, MAX-MIN produces nearly identical samples in some datasets, frequently making it hard for participants to choose between them. We show a per-dataset analysis of the results in Appendix A.

Runtime performance. Finally, we discuss the runtime performance of the algorithms on the Hidden Correlation dataset ($\sim 3.5M$), which is the largest one in our evaluation (Figure 14, right). We note that PAwS and MAX-MIN are the fastest among algorithms with reasonable perceptual efficacy. Their runtimes are similar, because they implement the same algorithm with modified objectives. While RANDOM and DBS are faster, they typically produce samples of poor perceptual quality. The KNN algorithm, which is used by DBS to identify points in sparse areas, dominates its running time, which stays constant across sample sizes. The runtimes of VAS and BLUE-NOISE are significantly longer, by 2–3 orders of magnitude. We note that VAS takes a long time to converge (~ 23 minutes for a sample of 250 points), but we have observed that it produces samples of similar quality after one pass over the data (~ 5 minutes for a sample of 250 points). Figure 14 reports both runtimes (till full convergence and for a single pass). We note that BLUE-NOISE is extremely inefficient (~ 3.6 hours for a sample of 250 points), which aligns with prior analyses [23, 84].

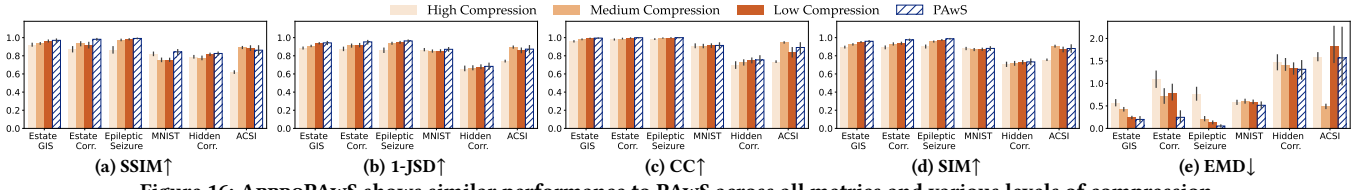


Figure 16: APPROPAwS shows similar performance to PAwS across all metrics and various levels of compression.

Key takeaways: PAwS robustly outperforms state-of-the-art sampling methods, with emphasized gains in smaller sample sizes. It is also orders of magnitude faster than the other state-of-the-art. Probabilistic methods have consistently low performance. While BLUE-NOISE often achieves good perceptual similarity, its runtime is prohibitive in large datasets. Diversity-based methods have more stable behavior and achieve similar performance to PAwS for large sample sizes, but VAS is again significantly slower. A user study further confirms that PAwS samples are frequently preferred by humans.

6.2 Performance of approximate visualization

In this section, we evaluate the effectiveness of approximate visualizations generated by APPROPAwS (Algorithm 2), using our perception-aware compression (Section 4.1). Compression splits the canvas area into non-overlapping bounding boxes based on two thresholds, λ and σ , controlling data approximation and homogeneity of perception weights, respectively. These parameters affect the level of compression: lower thresholds result in more and smaller boxes (lower compression), thus, sample points drawn randomly within a box match better the underlying data and lead to lower distortion (example in Figure 10a). We present results at three compression levels: (1) low: $\langle \lambda, \sigma \rangle = \langle 0.001, 0.001 \rangle$, (2) medium: $\langle \lambda, \sigma \rangle = \langle 0.002, 0.001 \rangle$, and (3) high: $\langle \lambda, \sigma \rangle = \langle 0.003, 0.01 \rangle$. For consistency and ease of exposition, we use the same threshold values for all datasets but ACSI. For ACSI, to observe notable differences across compression schemes, we vary the thresholds as: (1) low: $\langle \lambda, \sigma \rangle = \langle 0.001, 0.001 \rangle$, (2) medium: $\langle \lambda, \sigma \rangle = \langle 0.005, 0.001 \rangle$, and (3) high: $\langle \lambda, \sigma \rangle = \langle 0.01, 0.01 \rangle$. We emphasize that the derived representations may differ in the number of boxes: e.g., hidden correlation has 9,658, 4,042, and 993 boxes across the three levels (Figure 10a), while estate correlation has 3,491, 1,184, and 448 boxes. We include additional details in Appendix A. In practice, the thresholds can be tuned by data analysts using a grid search approach to reach the desired level of compression.

Figure 16 contrasts the perceptual quality of APPROPAwS samples at 3 compression levels with PAwS. We report the methods' similarity scores at sample size $k = 9,611$ —intuitively, distortion due to compression becomes more visible in larger sample sizes.

We note that APPROPAwS achieves excellent scores on the first four metrics, closely matching the performance of PAwS. We achieve high performance even at the highest compression level. Still, the trend that perceptual quality increases as compression decreases remains visible. We note that values better than PAwS are possible, though uncommon; we observe them on the ACSI dataset, which models a corner case in scatterplots, and the EMD metric, which is known in the literature to have less consistent behavior, and to be more difficult to optimize for, and “prefers sparser predictions, even if they do not perfectly align with fixated regions” [18].

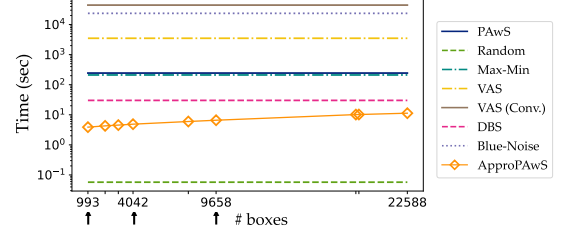


Figure 17: APPROPAwS is significantly more efficient than PAwS and state-of-the-art, even at low compression levels. ↑ marks the compression levels used in the results of Figure 16.

Runtime performance. Figure 17 demonstrates how the running time of APPROPAwS scales as compression decreases. We use the largest sample size ($k=9,611$) and largest dataset (hidden correlation) in our evaluation, to test 9 levels of compression, resulting in representations with 993 boxes, up to 22,588.

The running time of APPROPAwS increases with the number of boxes (as compression decreases), but not drastically. It is faster than all methods (except RANDOM, which has poor perceptual quality), and 100x faster than PAwS. Note that at 9,658 boxes (lowest compression in Figure 16), APPROPAwS produces approximate visualizations of high quality—comparable to PAwS but way faster. Intuitively, the gains in efficiency are higher in larger datasets and higher compression rates.

Key takeaways: APPROPAwS generates approximate visualizations with high perceptual similarity scores, comparable to PAwS, across various levels of compression, with running times up to 100x faster for large datasets.

7 Related Work

Sampling for visualization is a common approach for interactive visual analytics both in the visualization and database communities.

Scatterplots are a primary focus for sampling algorithms in the visualization community. According to a proposed taxonomy, different approaches can be characterized based on their end goal as: preserving (1) relative densities, (2) spatial separation and data shape, and (3) outliers [84, 107]. Density-oriented sampling methods aim to preserve relative density differences across areas in a visualization. Prior efforts include designing a non-uniform sampling method that models density in the data and pixel space [13, 14], modeling density via singular value decomposition (SVD) [50], using Z-order space-filling curves (a binning approach for kernel density estimation) [47, 110], or designing customized KD-tree structures to balance the selection of data points in different visualization areas [23]. Max-Min [35, 88], visualization-aware sampling [75], and blue noise sampling [106] are methods that optimize for spatial separation and data shape. We discussed these approaches in detail in Sections 1 and 6. In the visualization literature, outliers are defined

in multi-class scatterplots as the points whose class is different from the class of its neighbors [105]. A common strategy is to extend previously known methods to support this scenario [63, 103, 105]. Prior efforts though have not argued for directly modeling perception in sampling, which is a novel direction in our work, and our evaluation includes the state-of-the-art methods for single-class scatterplots that were found most effective in a recent user study [107].

Bars, pies, heat-maps, and lines charts are the focus of a lot of work in the database community [83]. Techniques primarily focus on sampling methods for approximate query processing (AQP) and incremental sampling [2, 5, 6, 20, 29, 38, 42, 45, 52, 70, 71, 87]. Typically the goal is to estimate an aggregate value with a desired confidence level. Thus, a common focus of these methods is estimating the number of samples needed to bound the estimation error. Alabi and Wu [6], the work closest to ours, use perceptual functions to estimate when the error becomes perceptually indiscernible for humans to improve sampling rates for approximate aggregation queries. Their work focuses on AQP and does not directly apply to scatterplots. We refer the reader to a survey for an in-depth review of related work for interactive and efficient data visualizations [83].

Information theory and probabilistic methods. Entropy and mutual information (MI) [15, 22, 33] have also been studied in the context of visualizations. The goal is to select a sample of points that preserve statistical associations among attributes of the original data. However, entropy and MI are both data-driven objectives targeting simulation and spatiotemporal data [15, 33]. There are also a few probabilistic sampling techniques used in the literature that use some level of randomization: stratified sampling, which divides the data set into non-overlapping groups based on some user-defined attribute and samples each group independently at random [9]; systematic sampling, which samples data points at a regular interval [65]; and clustering sampling, which, given a group of pre-defined clusters, randomly selects the clusters to be represented in a sample [46]. A major advantage of probabilistic sampling methods is they are easy to implement and computationally efficient. However, prior work has examined their limitations and highlighted the need for more sophisticated solutions [75].

Orthogonal approaches to sampling for improving the efficiency and usability of data visualization systems include data pre-fetching and pre-computation [10], designing specialized index structures for interactive visualizations [34, 41, 111], improving user experience and optimizing visualization design [27, 36, 55, 69, 84, 99], alternative data representations [51], and designing recommendation-based systems for data exploration and visualization [28, 40, 81, 82, 100].

Saliency maps and perception have seen interest in computer vision [94, 95] and natural language processing [16, 24]. However, data visualization does not always follow the rules of perception in the natural world [39], thus, improving on these models and adapting them to predict human focus in visualizations is an active problem in visualization research [54, 67, 96]. Saliency models for visualizations are still in their infancy but already demonstrate good performance at predicting attention-focus areas [67, 96]. We use the DVS model [67], which builds upon Itti et al. [49], as a black box. Future advances in visual perception tools can directly improve our methods through more effective saliency data.

8 Summary and Future Directions

In this paper, we introduce the problem of perception-aware sampling for scatterplot visualizations. We propose perception-augmented databases, which augment datasets with saliency information, and design novel sampling methodologies to derive perception-aware samples (PAwS) and approximate visualizations (APPROPAwS). Our evaluation demonstrated significant gains, both in the perceptual quality of the sample and sampling runtime.

Many interesting questions remain on targeting samples toward particular visual analysis tasks and optimizing samples to multiple target visualizations. On-the-fly sample augmentation can be useful to support interactivity in visualizations (e.g., when a user zooms in), and the biggest challenge is to achieve interactive sampling times. With the assistance of eye-tracking technologies, one may also aim for on-the-fly sample adaptation, based on user interactions and eye-gaze. Importantly, evaluating sampling methods in the context of visualizations is challenging, as there is no established benchmark. Creating such a benchmark would facilitate future research and make the comparison among different techniques easier and more robust.

References

- [1] Zeinab Abbasi, Vahab S. Mirrokni, and Mayur Thakur. 2013. Diversity Maximization Under Matroid Constraints. In *KDD '13*. 32–40.
- [2] Swarup Acharya, Phillip B Gibbons, and Viswanath Poosala. 1999. Aqua: A fast decision support systems using approximate query answers. In *Proceedings of the 25th International Conference on Very Large Data Bases*. 754–757.
- [3] Panos Achlioptas, Olga Diamanti, Ioannis Mitliagkas, and Leonidas Guibas. 2018. Learning representations and generative models for 3d point clouds. In *International conference on machine learning*. PMLR, 40–49.
- [4] Raghavendra Addanki, Andrew McGregor, Alexandra Meliou, and Zafeiria Moumoulioudou. 2022. Improved Approximation and Scalability for Fair Max-Min Diversification. In *25th International Conference on Database Theory (ICDT) (LIPICS, Vol. 220)*. Schloss Dagstuhl - Leibniz-Zentrum für Informatik, 7:1–7:21. <https://doi.org/10.4230/LIPIcs. ICDT.2022.7>
- [5] Sameer Agarwal, Barzan Mozafari, Aurojit Panda, Henry Milner, Samuel Madden, and Ion Stoica. 2013. BlinkDB: queries with bounded errors and bounded response times on very large data. In *Proceedings of the 8th ACM European conference on computer systems*. 29–42.
- [6] Daniel Alabi and Eugene Wu. 2016. Pfunk-h: Approximate query processing using perceptual models. In *Proceedings of the workshop on human-in-the-loop data analytics*. 1–6.
- [7] Robert Amar, James Eagan, and John Stasko. 2005. Low-level components of analytic activity in information visualization. In *IEEE Symposium on Information Visualization, 2005. INFOVIS 2005*. IEEE, 111–117.
- [8] Ralph G Andzejak, Klaus Lehnertz, Florian Mormann, Christoph Rieke, Peter David, and Christian E Elger. 2001. Indications of nonlinear deterministic and finite-dimensional structures in time series of brain electrical activity: Dependence on recording region and brain state. *Physical Review E* (2001).
- [9] Hirojiro Aoyama. 1954. A study of stratified random sampling. *Ann. Inst. Stat. Math* 6, 1 (1954), 1–36.
- [10] Leilani Battle, Remco Chang, and Michael Stonebraker. 2016. Dynamic prefetching of data tiles for interactive visualization. In *Proceedings of the 2016 International Conference on Management of Data*. 1363–1375.
- [11] Leilani Battle, Michael Stonebraker, and Remco Chang. 2013. Dynamic reduction of query result sets for interactive visualization. In *2013 IEEE International Conference on Big Data*. IEEE, 1–8.
- [12] Jon Louis Bentley. 1975. Multidimensional binary search trees used for associative searching. *Commun. ACM* 18, 9 (1975), 509–517.
- [13] Enrico Bertini and Giuseppe Santucci. 2004. By chance is not enough: preserving relative density through nonuniform sampling. In *Proceedings. Eighth International Conference on Information Visualisation, 2004. IV 2004*. IEEE, 622–629.
- [14] Enrico Bertini and Giuseppe Santucci. 2006. Give chance a chance: modeling density to enhance scatter plot quality through random data sampling. *Information Visualization* 5, 2 (2006), 95–110.
- [15] Ayan Biswas, Soumya Dutta, Han-Wei Shen, and Jonathan Woodring. 2013. An information-aware framework for exploring multivariate data sets. *IEEE Transactions on Visualization and Computer Graphics* 19, 12 (2013), 2683–2692.

[16] Corinna E Bonhage, Jutta L Mueller, Angela D Friederici, and Christian J Fiebach. 2015. Combined eye tracking and fMRI reveals neural basis of linguistic predictions during sentence comprehension. *Cortex* 68 (2015), 33–47.

[17] Allan Borodin, Aadhar Jain, Hyun Chul Lee, and Yuli Ye. 2017. Max-sum diversification, monotone submodular functions, and dynamic updates. *ACM Transactions on Algorithms (TALG)* 13, 3 (2017), 1–25.

[18] Zoya Bylinskii, Tilke Judd, Aude Oliva, Antonio Torralba, and Frédéric Durand. 2018. What do different evaluation metrics tell us about saliency models? *IEEE transactions on pattern analysis and machine intelligence* 41, 3 (2018), 740–757.

[19] Zoya Bylinskii, Adrià Recasens, Ali Borji, Aude Oliva, Antonio Torralba, and Frédéric Durand. 2016. Where should saliency models look next? In *Computer Vision–ECCV: 14th European Conference, Amsterdam, The Netherlands, October 11–14, 2016, Proceedings, Part V 14*. Springer, 809–824.

[20] Surajit Chaudhuri, Gautam Das, and Vivek Narasayya. 2007. Optimized stratified sampling for approximate query processing. *ACM Transactions on Database Systems (TODS)* 32, 2 (2007), 9–es.

[21] Min Chen and Amos Golan. 2015. What may visualization processes optimize? *IEEE transactions on visualization and computer graphics* 22, 12 (2015), 2619–2632.

[22] Min Chen and Heike Jänicke. 2010. An information-theoretic framework for visualization. *IEEE transactions on visualization and computer graphics* 16, 6 (2010), 1206–1215.

[23] Xin Chen, Tong Ge, Jian Zhang, Baoquan Chen, Chi-Wing Fu, Oliver Deussen, and Yunhai Wang. 2019. A recursive subdivision technique for sampling multi-class scatterplots. *IEEE transactions on visualization and computer graphics* 26, 1 (2019), 729–738.

[24] Kathy Conklin and Ana Pellicer-Sánchez. 2016. Using eye-tracking in applied linguistics and second language research. *Second Language Research* 32, 3 (2016), 453–467.

[25] Robert L. Cook. 1986. Stochastic sampling in computer graphics. *ACM Transactions on Graphics (TOG)* 5, 1 (1986), 51–72.

[26] Graham Cormode, Minos Garofalakis, Peter J Haas, Chris Jermaine, et al. 2011. Synopses for massive data: Samples, histograms, wavelets, sketches. *Foundations and Trends® in Databases* 4, 1–3 (2011), 1–294.

[27] Çağatay Demiralp, Michael S Bernstein, and Jeffrey Heer. 2014. Learning perceptual kernels for visualization design. *IEEE transactions on visualization and computer graphics* 20, 12 (2014), 1933–1942.

[28] Kyriaki Dimitriadou, Olga Papaemmanouil, and Yanlei Diao. 2016. AIDE: an active learning-based approach for interactive data exploration. *IEEE Transactions on Knowledge and Data Engineering* 28, 11 (2016), 2842–2856.

[29] Bolin Ding, Silu Huang, Surajit Chaudhuri, Kaushik Chakrabarti, and Chi Wang. 2016. Sample+ seek: Approximating aggregates with distribution precision guarantee. In *Proceedings of the 2016 International Conference on Management of Data*. 679–694.

[30] Frances Ding, Moritz Hardt, John Miller, and Ludwig Schmidt. 2021. Retiring adult: New datasets for fair machine learning. *Advances in neural information processing systems* 34 (2021), 6478–6490.

[31] Marina Drosou, Hosagrahar V Jagadish, Evangelia Pitoura, and Julia Stoyanovich. 2017. Diversity in big data: A review. *Big data* 5, 2 (2017), 73–84.

[32] Marina Drosou and Evangelia Pitoura. 2013. Diverse set selection over dynamic data. *IEEE Transactions on Knowledge and Data Engineering* 26, 5 (2013), 1102–1116.

[33] Soumya Dutta, Ayan Biswas, and James Ahrens. 2019. Multivariate pointwise information-driven data sampling and visualization. *Entropy* 21, 7 (2019), 699.

[34] Muhammad El-Hindi, Zheguang Zhao, Carsten Binnig, and Tim Kraska. 2016. Vistrees: fast indexes for interactive data exploration. In *Proceedings of the Workshop on Human-In-the-Loop Data Analytics*. 1–6.

[35] Yuval Eldar, Michael Lindenbaum, Moshe Porat, and Yehoshua Y Zeevi. 1997. The farthest point strategy for progressive image sampling. *IEEE transactions on image processing* 6, 9 (1997), 1305–1315.

[36] Geoffrey Ellis and Alan Dix. 2007. A taxonomy of clutter reduction for information visualisation. *IEEE transactions on visualization and computer graphics* 13, 6 (2007), 1216–1223.

[37] Haqiqing Fan, Hao Su, and Leonidas J Guibas. 2017. A point set generation network for 3d object reconstruction from a single image. In *Proceedings of the IEEE conference on computer vision and pattern recognition*. 605–613.

[38] Danyel Fisher, Igor Popov, Steven Drucker, and MC Schraefel. 2012. Trust me, I'm partially right: incremental visualization lets analysts explore large datasets faster. In *Proceedings of the SIGCHI conference on human factors in computing systems*. 1673–1682.

[39] Steven L Franconeri, Lace M Padilla, Priti Shah, Jeffrey M Zacks, and Jessica Hullman. 2021. The science of visual data communication: What works. *Psychological Science in the public interest* 22, 3 (2021), 110–161.

[40] Shaddy Garg, Subrata Mitra, Tong Yu, Yash Gadhia, and Arjun Kashettiwar. 2023. Reinforced approximate exploratory data analysis. In *Proceedings of the AAAI Conference on Artificial Intelligence*, Vol. 37. 7660–7669.

[41] Saheli Ghosh and Ahmed Eldawy. 2020. Aid*: a spatial index for visual exploration of geo-spatial data. *IEEE Transactions on Knowledge and Data Engineering* 34, 8 (2020), 3569–3582.

[42] Phillip B Gibbons and Yossi Matias. 1998. New sampling-based summary statistics for improving approximate query answers. In *Proceedings of the 1998 ACM SIGMOD international conference on Management of data*. 331–342.

[43] Lane Harrison, Fumeng Yang, Steven Franconeri, and Remco Chang. 2014. Ranking visualizations of correlation using weber's law. *IEEE transactions on visualization and computer graphics* 20, 12 (2014), 1943–1952.

[44] Christopher Healey and James Enns. 2011. Attention and visual memory in visualization and computer graphics. *IEEE transactions on visualization and computer graphics* 18, 7 (2011), 1170–1188.

[45] Joseph M Hellerstein, Ron Avnir, Andy Chou, Christian Hidber, Chris Olston, Vijayshankar Raman, Tali Roth, and Peter J Haas. 1999. Interactive data analysis: The control project. *Computer* 32, 8 (1999), 51–59.

[46] Ralph H Henderson and Thalanayarn Sundaresan. 1982. Cluster sampling to assess immunization coverage: a review of experience with a simplified sampling method. *Bulletin of the World Health Organization* 60, 2 (1982), 253.

[47] Ruizhen Hu, Tingkai Sha, Oliver Van Kaick, Oliver Deussen, and Hui Huang. 2019. Data sampling in multi-view and multi-class scatterplots via set cover optimization. *IEEE Transactions on Visualization and Computer Graphics* 26, 1 (2019), 739–748.

[48] Laurent Itti and Christof Koch. 2001. Computational modelling of visual attention. *Nature reviews neuroscience* 2, 3 (2001), 194–203.

[49] Laurent Itti, Christof Koch, and Ernst Niebur. 1998. A model of saliency-based visual attention for rapid scene analysis. *IEEE Transactions on pattern analysis and machine intelligence* 20, 11 (1998), 1254–1259.

[50] Paulo Joia, Fabiano Petronetto, and Luis Gustavo Nonato. 2015. Uncovering representative groups in multidimensional projections. In *Computer Graphics Forum*, Vol. 34. Wiley Online Library, 281–290.

[51] Daniel A Keim, Ming C Hao, Umeshwar Dayal, Halldor Janetzko, and Peter Bak. 2010. Generalized scatter plots. *Information Visualization* 9, 4 (2010), 301–311.

[52] Albert Kim, Eric Blais, Aditya Parameswaran, Piotr Indyk, Sam Madden, and Ronitt Rubinfeld. 2015. Rapid sampling for visualizations with ordering guarantees. In *Proceedings of the vldb endowment international conference on very large data bases*, Vol. 8. NIH Public Access, 521.

[53] Jang-Hyun Kim, Wonho Choo, and Hyun Oh Song. 2020. Puzzle Mix: Exploiting Saliency and Local Statistics for Optimal Mixup. In *Proceedings of the 37th International Conference on Machine Learning (Proceedings of Machine Learning Research, Vol. 119)*, Ha Daumé III and Aarti Singh (Eds.). PMLR, 5275–5285. <https://proceedings.mlr.press/v119/kim20b.html>

[54] Nam Wook Kim, Zoya Bylinskii, Michelle A Borkin, Krzysztof Z Gajos, Aude Oliva, Fredo Durand, and Hanspeter Pfister. 2017. Bubbleview: an interface for crowdsourcing image importance maps and tracking visual attention. *ACM Transactions on Computer-Human Interaction (TOCHI)* 24, 5 (2017), 1–40.

[55] Younghoon Kim and Jeffrey Heer. 2018. Assessing effects of task and data distribution on the effectiveness of visual encodings. In *Computer Graphics Forum*, Vol. 37. Wiley Online Library, 157–167.

[56] Matthias Kleindessner, Pranjal Awasthi, and Jamie Morgenstern. 2019. Fair k-center clustering for data summarization. In *International Conference on Machine Learning*. PMLR, 3448–3457.

[57] Bum Chul Kwon, Janu Verma, Peter J Haas, and Cagatay Demiralp. 2017. Sampling for scalable visual analytics. *IEEE computer graphics and applications* 37, 1 (2017), 100–108.

[58] Yann LeCun, Léon Bottou, Yoshua Bengio, and Patrick Haffner. 1998. Gradient-based learning applied to document recognition. *Proc. IEEE* 86, 11 (1998), 2278–2324.

[59] Christian Ledig, Lucas Theis, Ferenc Huszár, Jose Caballero, Andrew Cunningham, Alejandro Acosta, Andrew Aitken, Alykhan Tejani, Johannes Totz, Zehan Wang, et al. 2017. Photo-realistic single image super-resolution using a generative adversarial network. In *Proceedings of the IEEE conference on computer vision and pattern recognition*. 4681–4690.

[60] Sanghyeon Lee, Minkyu Jeon, Injae Kim, Yunyang Xiong, and Hyunwoo J Kim. 2022. SageMix: Saliency-Guided Mixup for Point Clouds. In *Advances in Neural Information Processing Systems*, S. Koyejo, S. Mohamed, A. Agarwal, D. Belgrave, K. Cho, and A. Oh (Eds.), Vol. 35. Curran Associates, Inc., 23580–23592. https://proceedings.neurips.cc/paper_files/paper/2022/file/9543942c237ded1b39b1fd37259ff88e-Paper-Conference.pdf

[61] Jia Li, Changqun Xia, Yafei Song, Shu Fang, and Xiaowu Chen. 2015. A data-driven metric for comprehensive evaluation of saliency models. In *Proceedings of the IEEE international conference on computer vision*. 190–198.

[62] Yiqun Lin, Lichang Chen, Haibin Huang, Chongyang Ma, Xiaoguang Han, and Shuguang Cui. 2022. Task-aware sampling layer for point-wise analysis. *IEEE Transactions on Visualization and Computer Graphics* (2022).

[63] Shixia Liu, Jianman Xiao, Junlin Liu, Xiting Wang, Jing Wu, and Jun Zhu. 2017. Visual diagnosis of tree boosting methods. *IEEE transactions on visualization and computer graphics* 24, 1 (2017), 163–173.

[64] Zhicheng Liu and Jeffrey Heer. 2014. The effects of interactive latency on exploratory visual analysis. *IEEE transactions on visualization and computer graphics* 20, 12 (2014), 2122–2131.

[65] William G Madow and Lillian H Madow. 1944. On the theory of systematic sampling, I. *The Annals of Mathematical Statistics* 15, 1 (1944), 1–24.

[66] Moeti M Masiane, Anne Driscoll, Wuchun Feng, John Wenskovitch, and Chris North. 2020. Towards insight-driven sampling for big data visualisation. *Behaviour & Information Technology* 39, 7 (2020), 788–807.

[67] Laura E Matzen, Michael J Haass, Kristin M Divis, Zhiyuan Wang, and Andrew T Wilson. 2017. Data visualization saliency model: A tool for evaluating abstract data visualizations. *IEEE transactions on visualization and computer graphics* 24, 1 (2017), 563–573.

[68] Adrian Mayorga and Michael Gleicher. 2013. Splatterplots: Overcoming overdraw in scatter plots. *IEEE transactions on visualization and computer graphics* 19, 9 (2013), 1526–1538.

[69] Luana Micalef, Gregorio Palmas, Antti Oulasvirta, and Tino Weinkauf. 2017. Towards perceptual optimization of the visual design of scatterplots. *IEEE transactions on visualization and computer graphics* 23, 6 (2017), 1588–1599.

[70] NG Minos and BG Philip. 2011. Approximate Query Processing: Taming the TeraBytes. *proceedings of SIGMOD* (2011).

[71] Dominik Moritz, Danyel Fisher, Bolin Ding, and Chi Wang. 2017. Trust, but verify: Optimistic visualizations of approximate queries for exploring big data. In *Proceedings of the 2017 CHI conference on human factors in computing systems*. 2904–2915.

[72] Zafeiria Moumouliou, Andrew McGregor, and Alexandra Meliou. 2021. Diverse Data Selection under Fairness Constraints. In *ICDT 2021*. 13:1–13:25.

[73] Jim Nilsson and Tomas Akenine-Möller. 2020. Understanding ssim. *arXiv preprint arXiv:2006.13846* (2020).

[74] Christopher R Palmer and Christos Faloutsos. 2000. Density biased sampling: An improved method for data mining and clustering. In *Proceedings of the 2000 ACM SIGMOD international conference on Management of data*. 82–92.

[75] Yongjoo Park, Michael Cafarella, and Barzan Mozafari. 2016. Visualization-aware sampling for very large databases. In *2016 IEEE 32nd International Conference on Data Engineering (ICDE)*. IEEE, 755–766.

[76] Emanuel Parzen. 1962. On estimation of probability density function and mode. *The annals of mathematical statistics* 33, 3 (1962), 1065–1076.

[77] Fabian Pedregosa, Gaël Varoquaux, Alexandre Gramfort, Vincent Michel, Bertrand Thirion, Olivier Grisel, Mathieu Blondel, Peter Prettenhofer, Ron Weiss, Vincent Dubourg, et al. 2011. Scikit-learn: Machine learning in Python. *the Journal of machine Learning research* 12 (2011), 2825–2830.

[78] Ofir Pele and Michael Werman. 2008. A linear time histogram metric for improved sift matching. In *Computer Vision–ECCV 2008: 10th European Conference on Computer Vision, Marseille, France, October 12–18, 2008, Proceedings, Part III* 10. Springer, 495–508.

[79] Ofir Pele and Michael Werman. 2009. Fast and robust earth mover’s distances. In *2009 IEEE 12th International Conference on Computer Vision*. IEEE, 460–467.

[80] R Doyle Portugal and Benat Fux Svaiter. 2011. Weber-Fechner law and the optimality of the logarithmic scale. *Minds and Machines* 21 (2011), 73–81.

[81] Vibhor Porwal, Subrata Mitra, Fan Du, John Anderson, Nikhil Sheoran, Anup Rao, Tung Mai, Gautam Kowshik, Saphotharan Nair, Sameeksha Arora, et al. 2022. Efficient Insights Discovery through Conditional Generative Model based Query Approximation. In *Proceedings of the 2022 International Conference on Management of Data*. 2397–2400.

[82] Xin Qian, Ryan A Rossi, Fan Du, Sungchul Kim, Eunyee Koh, Sana Malik, Tak Yeon Lee, and Joel Chan. 2021. Learning to recommend visualizations from data. In *Proceedings of the 27th ACM SIGKDD Conference on Knowledge Discovery & Data Mining*. 1359–1369.

[83] Xuedi Qin, Yuyu Luo, Nan Tang, and Guoliang Li. 2020. Making data visualization more efficient and effective: a survey. *The VLDB Journal* 29, 1 (2020), 93–117.

[84] Ghulam Jilani Quadri, Jennifer Adorno Nieves, Brenton M Wiernik, and Paul Rosen. 2022. Automatic scatterplot design optimization for clustering identification. *IEEE Transactions on Visualization and Computer Graphics* (2022).

[85] Ghulam Jilani Quadri and Paul Rosen. 2020. Modeling the influence of visual density on cluster perception in scatterplots using topology. *IEEE Transactions on Visualization and Computer Graphics* 27, 2 (2020), 1829–1839.

[86] Ghulam Jilani Quadri and Paul Rosen. 2021. A survey of perception-based visualization studies by task. *IEEE transactions on visualization and computer graphics* 28, 12 (2021), 5026–5048.

[87] Sajjadur Rahman, Maryam Aliakbarpour, Ha Kyung Kong, Eric Blais, Karrie Karahalios, Aditya Parameswaran, and Ronitt Rubinfield. 2017. I’ve seen “enough” incrementally improving visualizations to support rapid decision making. *Proceedings of the VLDB Endowment* 10, 11 (2017), 1262–1273.

[88] S. S. Ravi, D. J. Rosenkrantz, and G. K. Tayi. 1994. Heuristic and Special Case Algorithms for Dispersion Problems. *Oper. Res.* 42, 2 (April 1994), 299–310.

[89] Adria Recasens, Petr Kellnhofer, Simon Stent, Wojciech Matusik, and Antonio Torralba. 2018. Learning to zoom: a saliency-based sampling layer for neural networks. In *Proceedings of the European conference on computer vision (ECCV)*. 51–66.

[90] Ronald A Rensink and Gideon Baldridge. 2010. The perception of correlation in scatterplots. In *Computer graphics forum*, Vol. 29. Wiley Online Library, 15

[91] Julian A Ramos Rojas, Mary Beth Kery, Stephanie Rosenthal, and Anind Dey. 2017. Sampling techniques to improve big data exploration. In *2017 IEEE 7th symposium on large data analysis and visualization (LDAV)*. IEEE, 26–35.

[92] Alper Sarikaya and Michael Gleicher. 2017. Scatterplots: Tasks, data, and designs. *IEEE transactions on visualization and computer graphics* 24, 1 (2017), 402–412.

[93] David W Scott. 2015. *Multivariate density estimation: theory, practice, and visualization*. John Wiley & Sons.

[94] Karthikeyan Shanmuga Vadivel, Thuyenn Ngo, Miguel Eckstein, and BS Manjunath. 2015. Eye tracking assisted extraction of attentionally important objects from videos. In *Proceedings of the IEEE Conference on Computer Vision and Pattern Recognition*. 3241–3250.

[95] Ran Shi, Ngı King Ngan, and Hongliang Li. 2017. Gaze-based object segmentation. *IEEE Signal Processing Letters* 24, 10 (2017), 1493–1497.

[96] Sungbok Shin, Sunghyu Chung, Sanghyun Hong, and Niklas Elmquist. 2022. A scanner deeply: Predicting gaze heatmaps on visualizations using crowdsourced eye movement data. *IEEE Transactions on Visualization and Computer Graphics* 29, 1 (2022), 396–406.

[97] Ben Shneiderman. 1984. Response time and display rate in human performance with computers. *ACM Computing Surveys (CSUR)* 16, 3 (1984), 265–285.

[98] Bernard W Silverman. 2018. *Density estimation for statistics and data analysis*. Routledge.

[99] Danielle Albers Szafir. 2017. Modeling color difference for visualization design. *IEEE transactions on visualization and computer graphics* 24, 1 (2017), 392–401.

[100] Manasi Vartak, Sajjadur Rahman, Samuel Madden, Aditya Parameswaran, and Neoklis Polyzotis. 2015. Seedb: Efficient data-driven visualization recommendations to support visual analytics. In *Proceedings of the VLDB Endowment International Conference on Very Large Data Bases*, Vol. 8. NIH Public Access, 2182.

[101] Yue Wang, Alexandra Meliou, and Jerome Miklau. 2018. Rc-index: Diversifying answers to range queries. *Proceedings of the VLDB Endowment* 11, 7 (2018), 773–786.

[102] Zhou Wang, Alan C Bovik, Hamid R Sheikh, and Eero P Simoncelli. 2004. Image quality assessment: from error visibility to structural similarity. *IEEE transactions on image processing* 13, 4 (2004), 600–612.

[103] Li-Yi Wei. 2010. Multi-class blue noise sampling. *ACM Transactions on Graphics (TOG)* 29, 4 (2010), 1–8.

[104] Tong Wu, Liang Pan, Junzhe Zhang, Tai Wang, Ziwei Liu, and Dahua Lin. 2021. Density-aware chamfer distance as a comprehensive metric for point cloud completion. *arXiv preprint arXiv:2111.12702* (2021).

[105] Shouxing Xiang, Xi Ye, Jiazhai Xia, Jing Wu, Yang Chen, and Shixia Liu. 2019. Interactive correction of mislabeled training data. In *2019 IEEE Conference on Visual Analytics Science and Technology (VAST)*. IEEE, 57–68.

[106] Dong-Ming Yan, Jian-Wei Guo, Bin Wang, Xiao-Peng Zhang, and Peter Wonka. 2015. A survey of blue-noise sampling and its applications. *Journal of Computer Science and Technology* 30, 3 (2015), 439–452.

[107] Jun Yuan, Shouxing Xiang, Jiazhai Xia, Lingyun Yu, and Shixia Liu. 2020. Evaluation of sampling methods for scatterplots. *IEEE Transactions on Visualization and Computer Graphics* 27, 2 (2020), 1720–1730.

[108] Richard Zhang, Phillip Isola, Alexei A Efros, Eli Shechtman, and Oliver Wang. 2018. The unreasonable effectiveness of deep features as a perceptual metric. In *Proceedings of the IEEE conference on computer vision and pattern recognition*. 586–595.

[109] Hang Zhao, Orazio Gallo, Iuri Frosio, and Jan Kautz. 2016. Loss functions for image restoration with neural networks. *IEEE Transactions on computational imaging* 3, 1 (2016), 47–57.

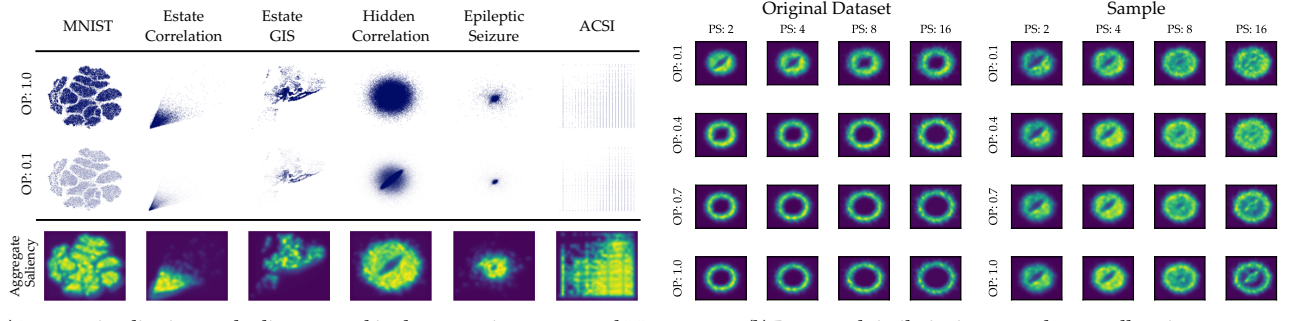
[110] Yan Zheng, Jeffrey J. Estes, Jeff M Phillips, and Feifei Li. 2013. Quality and efficiency for kernel density estimates in large data. In *Proceedings of the 2013 ACM SIGMOD International Conference on Management of Data*. 433–444.

[111] Kostas Zoumpatianos, Stratos Idreos, and Themis Palpanas. 2014. Indexing for interactive exploration of big data series. In *Proceedings of the 2014 ACM SIGMOD international conference on Management of data*. 1555–1566.

A Appendix

Overview of experimental design. Figure 18 provides an overview of the experimental design choices we described in Section 6 of the main paper. We show the aggregate saliency maps derived using our approach and describe in more detail our methodology for computing perceptual similarity. Figure 19 shows the perception weights for the datasets in our evaluation, assigning a higher perception value to highly salient or highly dense areas.

Perceptual similarity metrics. Figure 20 shows extensive results about the behavior of different sampling methods across six datasets



(a) Dataset visualizations and saliency stored in the perception-augmented DB

(b) Perceptual similarity is averaged across all settings

Figure 18: (a) Visualizations of the datasets we use in the experimental evaluation and their aggregate saliency maps. (b) We demonstrate the evaluation methodology on the hidden correlation dataset. We render the original dataset using 16 configurations by varying the opacity (OP) and point size (PS) and generate the saliency maps using DVS [67] (left). Given a sample, we use the same configurations to generate 16 saliency maps for the sample (right). We compare the saliency similarity of each pair (original and sample) with the same configuration, and compute the final perceptual similarity as the average across all 16 configurations.

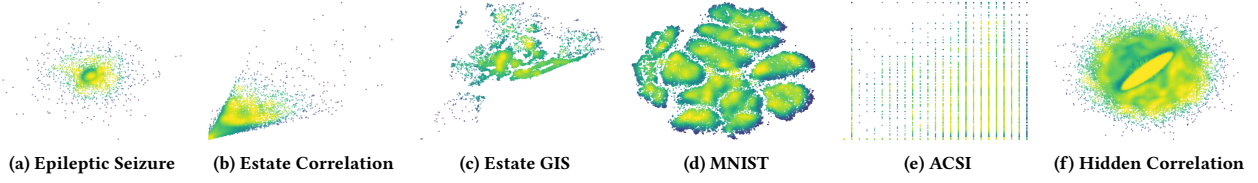


Figure 19: Perception weights for the datasets in our experimental evaluation.

and five evaluation metrics introduced in Section 5 of the main paper. The observations we make are consistent with the discussion in Section 6, and different metrics show similar results. PAwS has strong behavior across all datasets and metrics, while probabilistic-based approaches consistently underperform. MAX-MIN and VAs typically perform better as the sample size increases. The behavior of BLUE-NOISE varies across datasets, while in hidden correlation performs as poorly as probabilistic-based methods with extremely low scores in SIM, CC, and 1-JSD metrics. We note EMD is a difficult metric to optimize for, and in some datasets (i.e., in epileptic seizure) all sampling methods reach lower scores.

Qualitative samples and user study results per dataset. Figure 21 shows the visualizations we used in our user study assessing the efficacy of different sampling methods across three key aspects: (1) preserving density variations, (2) retaining outliers and overall data shape, and (3) maintaining correlation trends, clusters, and other patterns. Figures 22, 23, and 24 show the results per dataset and sampling pair—comparing a PAwS sample to an alternative sample—across these three key criteria. Figure 25 shows the result for the best overall sample per dataset. We observe PAwS is frequently preferred by humans compared to state-of-the-arts methods, while the preference becomes more evident in datasets where other sampling methods fail to represent some trend in the data; for instance, in hidden correlation, PAwS is overly favored compared to all other methods, which fail to represent both the correlation trend and the overall data distribution. Similarly, in ACSI, humans overly prefer PAwS compared to probabilistic-based approaches that create an evident “gap” in the sample.

Compression schemes and APPROPAwS samples. We report additional results for APPROPAwS (Algorithm 2), which is our method for approximate visualizations. APPROPAwS uses perception-aware

compressed data representations to derive samples without having access to the original data. Our compression approach (Section 4) uses two thresholds, λ and σ , to derive these data representations and splits the canvas into non-overlapping bounding boxes that sufficiently approximate the data in them (as guided by λ), and cover areas of similar perception weights (as guided by σ). Then APPROPAwS creates a sample by selecting points uniformly at random from these boxes. Lower values for the thresholds result in representations with a higher number of boxes that closely represent the underlying data (lower compression), and thus, the level of distortion observed in an APPROPAwS sample is lower.

We present results at three compression levels: (1) low: $\langle \lambda, \sigma \rangle = \langle 0.001, 0.001 \rangle$, (2) medium: $\langle \lambda, \sigma \rangle = \langle 0.002, 0.001 \rangle$, and (3) high: $\langle \lambda, \sigma \rangle = \langle 0.003, 0.01 \rangle$. For consistency and ease of exposition, we use the same threshold values for all datasets but ACSI. For ACSI, to observe notable differences across compression schemes, we vary the thresholds as: (1) low: $\langle \lambda, \sigma \rangle = \langle 0.001, 0.001 \rangle$, (2) medium: $\langle \lambda, \sigma \rangle = \langle 0.005, 0.001 \rangle$, and (3) high: $\langle \lambda, \sigma \rangle = \langle 0.01, 0.01 \rangle$. Figure 26 shows the derived compression schemes, and Figure 27 shows samples, across three sampling sizes, derived by APPROPAwS while using the corresponding data representations. We observe that qualitative degradation becomes more visible in high compression schemes, but APPROPAwS still captures the main trends and shape of the datasets.

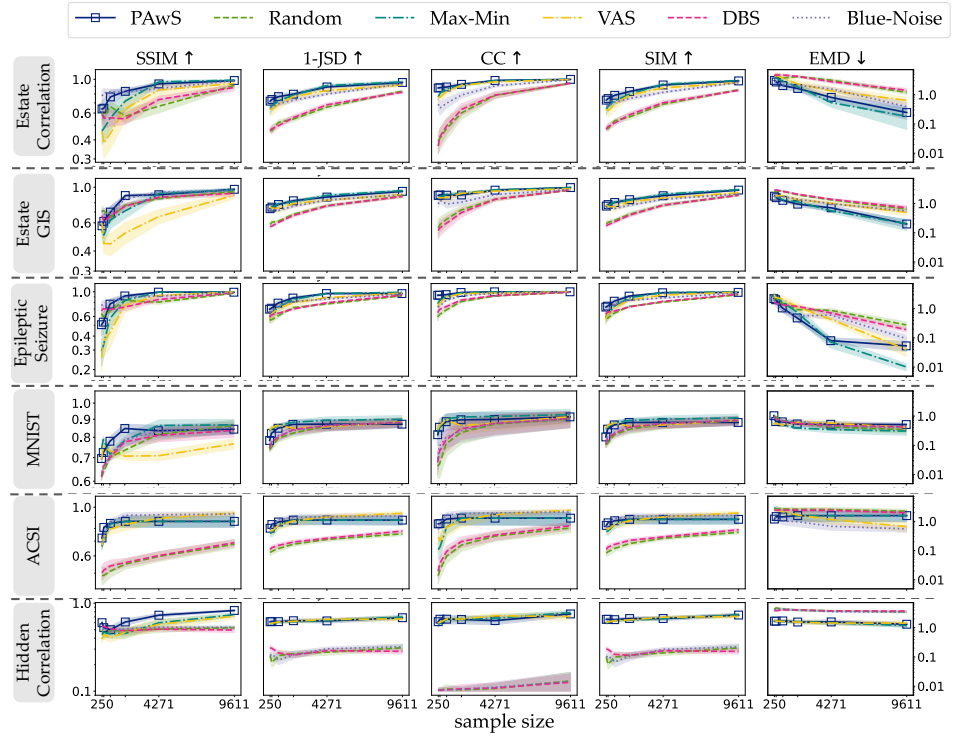


Figure 20: Experimental results across all datasets and metrics.

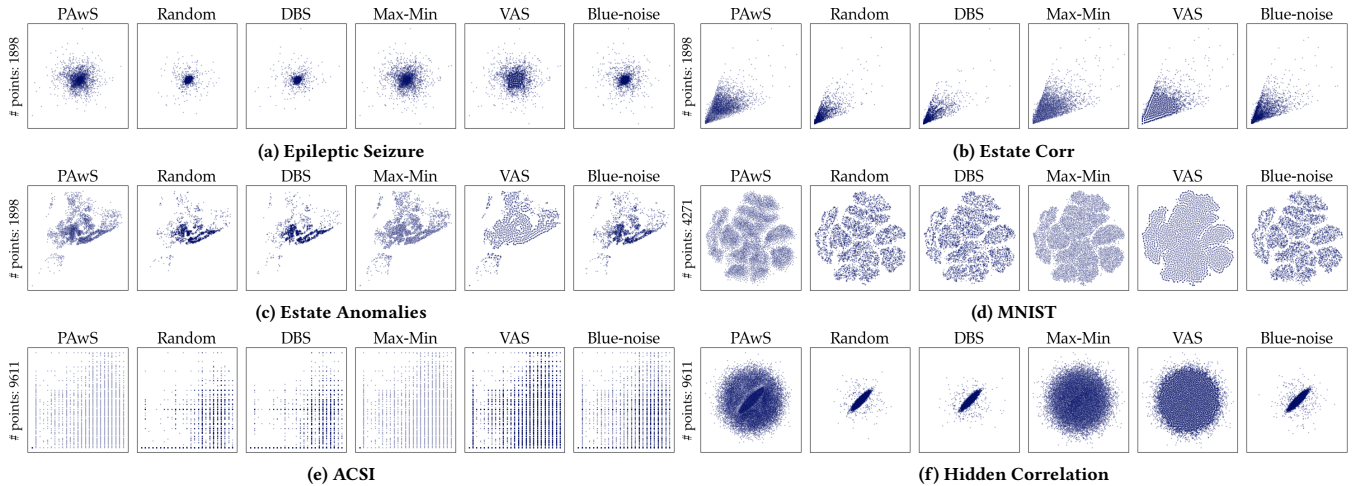


Figure 21: Visual stimuli used in the user study experiments for all datasets and sampling methods.

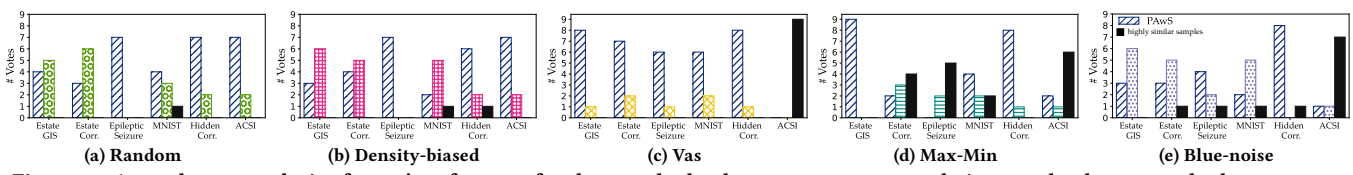
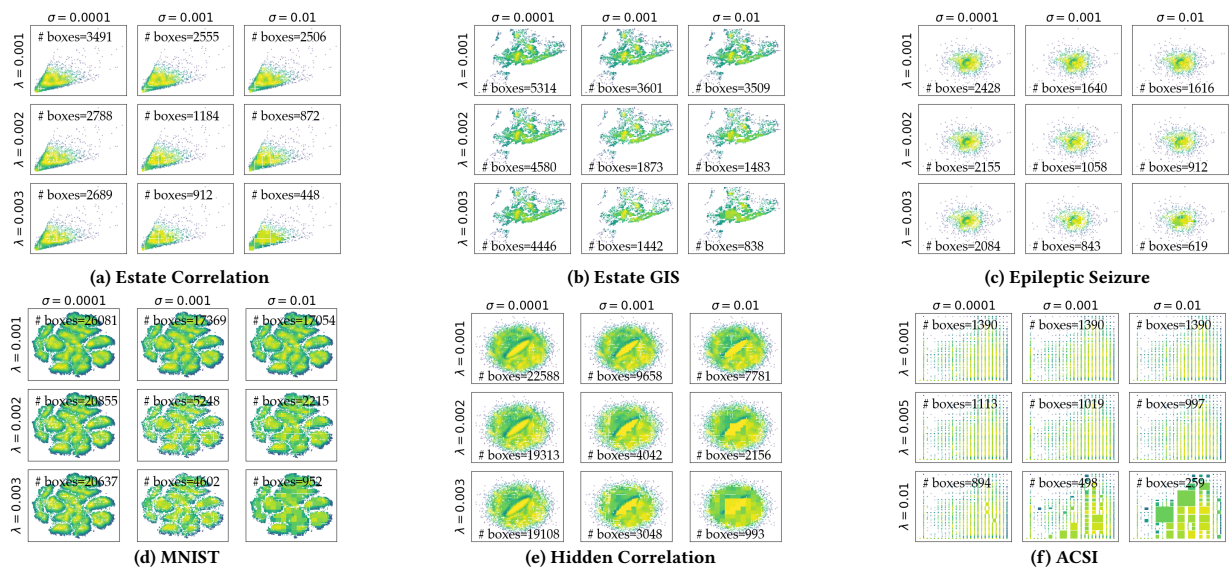
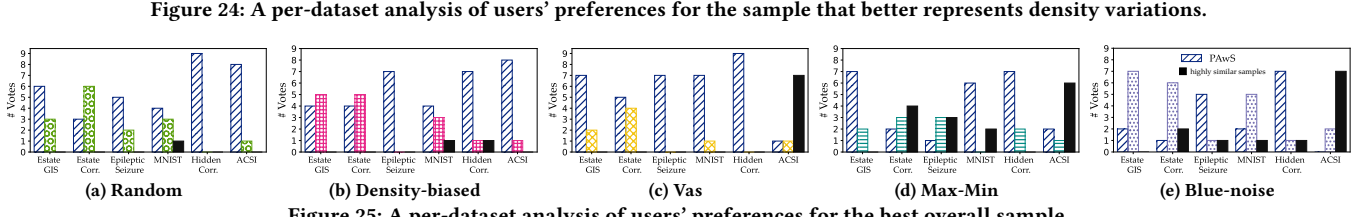
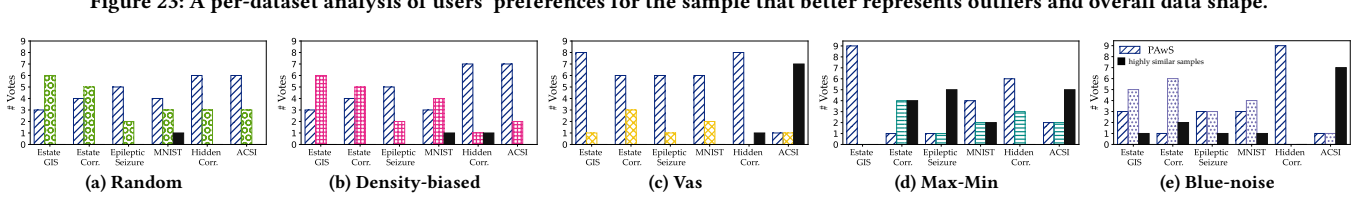
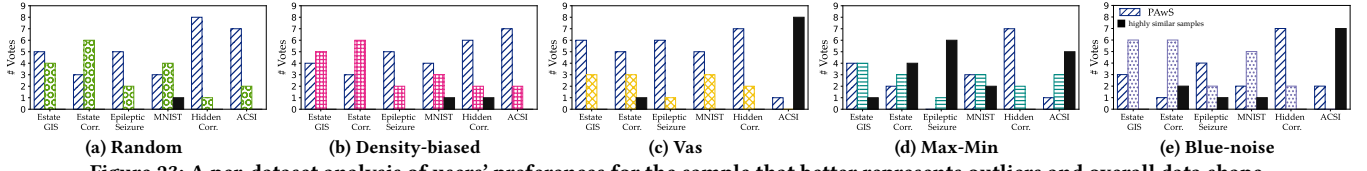


Figure 22: A per-dataset analysis of users' preferences for the sample that better represents correlation trends, clusters, and other patterns.



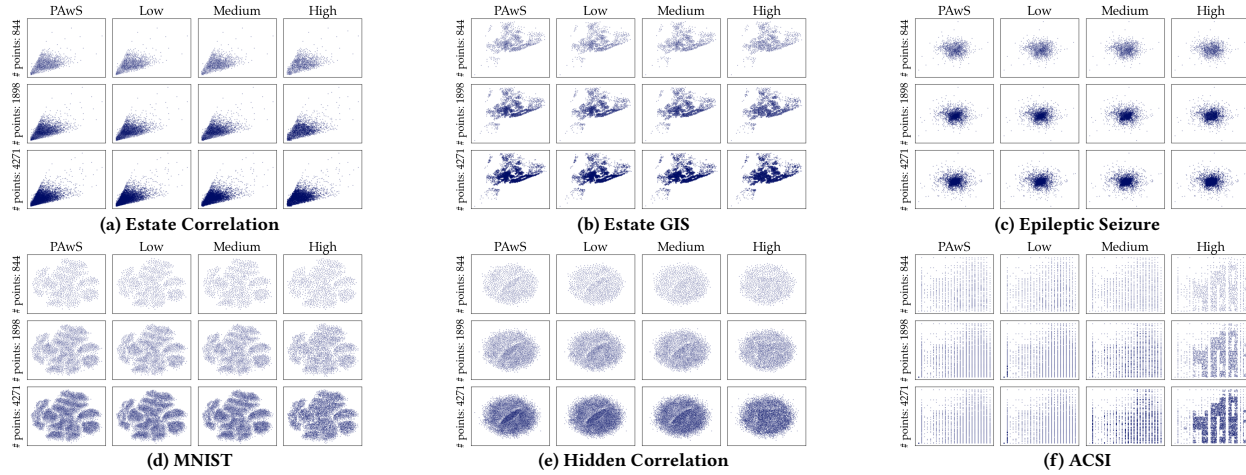


Figure 27: Approximate visualizations of various sample sizes, as derived by APPROPAwS using three perception-aware compressed data representations. We show results for three levels of compression for the various datasets.